2002

Buckling analysis of grid stiffened composite structures

Samuel Kidane
Louisiana State University and Agricultural and Mechanical College, skidane@lsu.edu

BUCKLING ANALYSIS OF GRID STIFFENED COMPOSITE STRUCTURES

A Thesis

Submitted to the Graduate Faculty of the
Louisiana State University and
Agricultural and Mechanical College
in partial fulfillment of the
requirements for the degree of
Master of Science in Mechanical Engineering

in

The Department of Mechanical Engineering

By
Samuel Kidane
B.Sc., Addis Ababa University, 1997
August 2002

ACKNOWLEDGEMENTS

I would first like to thank my parents, B/G Kidane Teklu and W/o Tsegaberhan Sebhatu as well as my sisters Eden Kidane and Nardos Kidane for their unconditional love and constant support throughout my studies. I owe all my achievements to them.

I would also like to express my sincere gratitude to my major professor Dr. Eyassu Woldesenbet for his advice and guidance throughout this research project. My gratitude also goes to my committee members Dr. Su-Seng Pang, Dr. Jack E. Helms, and Dr. Guoqiang Li for their sincere advice and encouragement. Special thanks goes to Dr. Guoqiang Li for dedicating so much time to helping me with my research and making the timely completion of my thesis possible.

In addition, I would like to thank Rajesh Krithivasan for helping me with my finite elements and ANSYS queries. Much thanks also goes out to Nikhil Gupta from whom I learned so much. I would like to thank Sarah Benoit and all my friends who stood by me and offered their support in every way.

Last but not least, I would like to thank Diane Morgan, who, no matter how busy, was always nice, concerned and helpful.

TABLE OF CONTENTS

LIST OF TABLES

LIST OF FIGURES

ABSTRACT

Buckling of a stiffened composite cylinder is a very complex phenomenon that involves complex interactions between the skin and the stiffeners. Depending on different configurations of the skin and stiffener, different buckling failure modes and failure loads are observed in stiffened cylinders. In this work failure modes and buckling loads of stiffened composite cylinders under uniaxial loading condition is investigated by using analytical and experimental approaches.

In the first Chapter an improved smeared method is developed to model the buckling problem of an isogird stiffened composite cylinder. In this model the stiffness contributions of the stiffeners is computed by analyzing the moment and force effect of the stiffener on a unit cell. Then the equivalent stiffness of the stiffener/shell panel is computed by superimposing the stiffness contribution of the stiffeners and the shell. Once the equivalent stiffness parameters are determined for the whole panel, the buckling load is calculated using the energy method.

A 3-D finite-elements model was also built which takes into consideration the exact geometric configuration and the orthotropic properties of the stiffeners and the shell. Based on the finite-elements model a discussion was made on the different buckling failure modes observed.

A limited experimental analysis was also performed to compliment the two analytical methods used to determine the buckling load of the stiffened cylinder. Results of the three types of analysis methods are compared, and comments made on the reliability of the analytical models developed. Finally a parametric study was carried out and general conclusions were drawn regarding the optimum configurations of the different parameters of the grid-stiffened cylinder.

1. INTRODUCTION

Structural efficiency is a primary concern in today's aerospace and aircraft industries. This brings about the need for strong and light weight materials. Due to their high specific strength, fiber reinforced polymers find wide application in these areas. Cylindrical structures made of composite material are widely used in the above mentioned industries. Aircraft fuselage, and launch vehicle fuel tanks are some of the many applications of these structures in aerospace and aircraft industries [1].

Grid stiffened cylinders are cylinders having a certain kind of stiffening structures either on the inner, outer or both sides of the shell. Having stiffeners significantly increases the load resistance of a cylinder without much increase in weight. To further reduce the weight, both the shell and the stiffeners are made with fiber-reinforced polymers. The stiffening structure can have a simple ring and stringer arrangement or a more complex isogrid pattern. The optimum type of stiffener configuration is dictated by the type of application, the loading condition, cost, and other factors. The advent of new manufacturing techniques in filament winding and automated fiber placement techniques as well as new innovative tooling concepts have decreased the manufacturing difficulties and hence have boosted the application of these grid stiffened composite cylinders [2,3]. The promising future of stiffened composite cylinders has in turn led to an extensive research work in this area [1-8].

Cylindrical shells are subjected to any combination of in plane, out of plane and shear loads during application. Due to the geometry of these structures, buckling is one of the most important failure criteria. Buckling failure mode of a stiffened cylindrical shell can further be subdivided into global buckling, local skin buckling and stiffener crippling. Global buckling is collapse of the whole structure, i.e. collapse of the stiffeners and the shell as one unit. Local skin

buckling and stiffeners crippling on the other hand are localized failure modes involving local failure of only the skin in the first case and the stiffener in the second case. A grid stiffened cylinder will fail in any of these failure modes depending on the stiffener configuration, skin thickness, shell winding angle and type of applied load. Several methods have so far been developed to predict the different buckling loads and mode shapes of stiffened cylinders. The different approaches in different literatures can broadly be classified as the discrete method, the branched shell and plate approach and the smeared stiffeners approach [4].

In this master's thesis, an analytical model was developed for prediction of buckling load of a grid stiffened composite cylinder subjected to uniaxial loading condition. The smeared stiffener approach was used to develop the analytical model. The model developed is more general in the sense that any configuration of stiffeners, on either one side or both sides of the shell can be modeled accurately. Stiffened cylinders having either symmetrical or unsymmetrical shell laminates can also be modeled with equal ease using this model. A 3-D finite-elements model was also built using ANSYS finite-elements software to gauge the accuracy of the closed form solutions obtained. Due to the expensive nature of grid stiffened composite cylinder test specimens, extensive experimentation could not be performed. But the results of the few experiments done are included for comparison purposes. The three methods used to investigate the buckling phenomena of stiffened composite cylinders were compared with each other and differences observed were accounted for. The main goal in any structural design problem is optimization of the different parameters involved. Hence a full chapter has been devoted at the end of this thesis for parametric study and optimization.

2. LITERATURE REVIEW

Over the past four decades, a lot of research has been focused on the buckling, collapse, and post buckling behavior of cylindrical shells [9]. A good portion of this work was devoted to the study of stiffened cylinders. The simplest stiffened cylinder consists of only axial stiffeners or stringers. A ring structure can be added to the stringers to achieve a better stiffened orthogrid configuration. A work by Graham [10] presents analysis method for determining the buckling loads of ring and stringer stiffened cylinders. Another type of stiffener arrangement is the cross stiffeners arrangement. This results in diamond shaped pattern of stiffeners. Phillips and Gurdal, in their work titled "Structural Analysis and Optimum Design of Geodesically Stiffened Composite Panels" discuss a smearing method for determining the global buckling load of this type of stiffened panels [5]. Isogrid stiffened cylinders, which this thesis paper mainly deals with, consists of cross stiffeners at $\pm 60^{o}$ and horizontal stiffeners. This arrangement results in equilateral triangle grid pattern of stiffener. From research works previously performed isogrid cylinders are in general found to be more efficient than orthogrid cylinder [1].

Different analytical tools have so far been developed by researches to successfully predict the three buckling failure modes associated with stiffened cylinders subjected to different loading conditions. These analytical tools developed, as mentioned in the introduction are divided into three major categories.

The discrete method models stiffeners as lines of axial bending and torsional stiffness on the skin. This approach can be difficult to use when the panel is stiffened in more than two directions or when the stiffeners are not symmetric about the skin mid-surface, however can be quite useful for simpler stiffener arrangements. The work done by Wang et. al. titled "Discrete analysis of stiffened composite cylindrical shells" is a good example of this type of analysis [8].

The branched plate and shell method is the second approach for building analytical models of grid stiffened composite cylinders. This approach is more flexible and more accurate and usually involves the use of finite-elements modeling. The use of finite-elements analysis for investigation of buckling problem of composite cylinders is becoming popular due to the improvement in computational hardware and emergence of highly specialized software. Depending on the degree of accuracy desired and limit of computational cost, three types of buckling analysis can be carried out. Linear bifurcation analysis is the basic analysis type which does not take into consideration the prebuckling deformation and stresses. This analysis can accurately predict the buckling load of a geometrically perfect compression loaded cylinder, and the prebuckling deformation and stress in the cylinder have an insignificant effect on the predicted bifurcation buckling load of the shell [11]. The second kind of bifurcation analysis takes into consideration the nonlinear prebuckling deformation and stresses and results in a much more accurate buckling loads. The third analysis, the nonlinear buckling analysis, allows for large nonlinear geometric deflections. Unlike the previous two bifurcation analyses that are eignevalue problems, the nonlinear analysis is iterative in nature. In this analysis the load is steadily increased until the solution starts to diverge [12]. A lot of work has been done in finite-elements analysis pertaining to the investigation of buckling of stiffened cylinders [11,13]. One of the major drawbacks associated with this tool is the tedious model-building phase involved and the subsequent inconvenient parametric study.

The third type of analytical modeling method, the smeared stiffener approach uses a mathematical model to smear the stiffeners into an equivalent laminate and determine the equivalent orthotropic stiffness of the laminate and determine the equivalent orthotropic stiffness of the laminate. A smeared stiffener theory that accounts for the skin-stiffener interaction was

developed by Narvin *et al*. [4]. In this work, a method is presented for the derivation of neutral surface profile of the grid/shell assembly by using minimum potential energy principle and static conditions. However, this analysis was developed for a symmetric shell laminate and assumes a semi-infinite stiffened flat panel. Another work using the smeared approach was done by Phillips and Gurdal [5]. They analyzed the forces on a unit cell that represented the whole grid network and came up with equivalent stiffness parameters of the whole panel. The model developed was limited in the sense that it was restricted to symmetric panels, i.e., panels stiffened on both faces.

Another area of interest for researchers studying buckling problems of cylinders is the effect of imperfections on the buckling load of cylinders. The work done by Riddick and Hyder [13], is one of the many papers published on this topic. These authors examined the effect of measured imperfections on the buckling and post buckling response characteristics of circular cylinders constructed of four distinct circumferential segments. In this work the authors state that the measured imperfections have an influence on the postbuckling response of the axially-stiff cylinders, but not on the circumferentially–stiff one [13].

Optimization of grid stiffened composite cylinders is also an area of interest to many researchers. Narvin, Norman & Damodar have worked on optimizations of grid stiffened composite panels [7] as well as general stiffened composite circular cylinders [1]. In both works they have considered all the three modes of buckling failure modes. They have used genetic algorithm discrete optimization. In their study they considered design variables like axial and transverse stiffener spacing, stiffener height and thickness skin laminate and stiffening configuration.

A great amount of work has so far been done in the area of shell instability problems that it makes it hard to mention all. The above research efforts discussed in this section are some of

the works the author considers relevant to the research presented in this thesis. Reference [9] presents a relatively comprehensive summery of works performed in cylindrical shell buckling problems and can be referred for further information.

3. ANALYTICAL MODEL

It is first required to determine the equivalent extensional, coupling and bending matrices (A, B and D matrices respectively) of the overall stiffened cylinder in order to calculate the global buckling load of the structure. This involves determining the stiffness contribution of the grid (stiffener) as well as the shell. In this Chapter a smeared method is developed to determine the equivalent stiffness parameters of the panel. The smeared method is a way of reducing the stiffener/shell structure into an equivalent laminate. A detailed outline of the steps followed to develop the analytical model and the assumptions made are presented below.

In developing the analytical model, a unit cell of the stiffener structure has to be defined first. The unit cell is chosen such that the whole grid structure can be reproduced by repetition of this unit cell (Fig. 1).

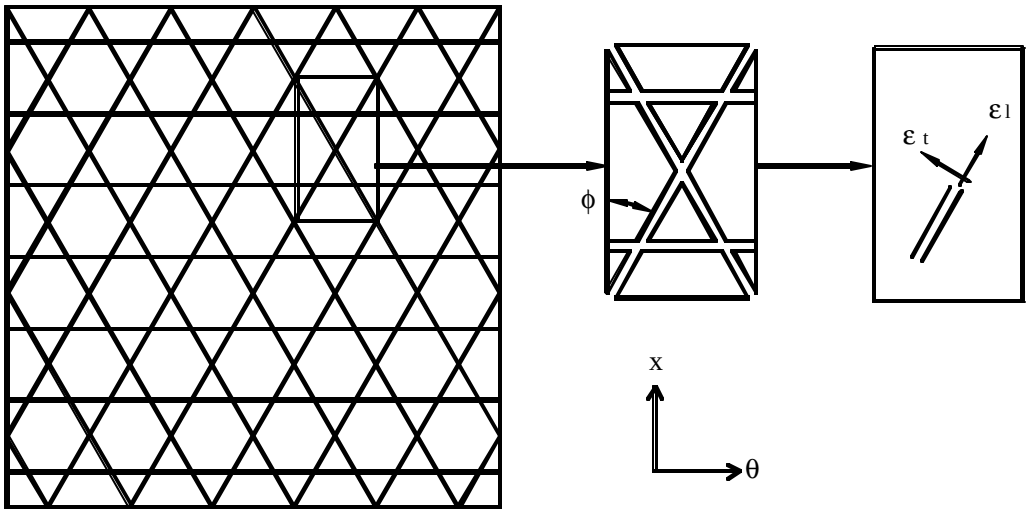

Figure 1. Unit cell and coordinate system.

The equivalent stiffness parameters of this unit cell are determined and then applied to the whole cylinder panel. This is valid as the whole panel can be generated from this unit cell. In determining the stiffness contribution of the stiffeners to the total structure, the force and moment interaction of the stiffeners and the shell needs to be analyzed. The overall stiffness of

the panel is then computed by superimposing the stiffener and the shell stiffness parameters according to the volume fraction of each. In order to carry out the superposition of the A, B and D matrix of the shell and stiffeners, the constitutive equation developed for the stiffeners needs to be a function of the mid plane strains and curvatures of the shell. In developing this analytical model, the following assumptions are made.

1. The transverse modulus of the unidirectional stiffeners is much lower than the longitudinal modulus, and the cross sectional dimensions are also very small compared to the length dimension, therefore the stiffeners are assumed to support axial load only.
2. The strain is uniform across the cross sectional area of the stiffeners. Hence a uniform stress distribution is assumed.
3. Load is transferred through shear forces between the stiffeners and the shell.

3.1. Force Analysis

The mid plane strains and curvatures of the shell are given by e_x^o, e_q^o, e_{xq}^o and k_x, k_q, k_{xq} respectively. The corresponding strains on the inner surface of the shell (the interface of the stiffener and the shell) are given in terms of the mid plane strains and curvatures by Equation (1) [14]. Since the stiffeners are attached to the skin at this interface, the strains at this interface are used as the matching condition for the stiffener and the shell.

$$\begin{aligned} e_x &= e_x^o + k_x(t/2) \\ e_q &= e_q^o + k_q(t/2) \\ e_{xq} &= e_{xq}^o + k_{xq}(t/2) \end{aligned} \qquad (1)$$

Where t is the thickness of the shell. The strains obtained by Equation (1) need to be resolved along the stiffeners directions since these are the relevant strains. This is done by premultiplying the interface strains by the transformation matrix Equation (2) [15]. This results in strains along

the stiffener direction e_l, normal to the stiffener directions e_t and corresponding shear strain e_{lt} (Fig. 1).

$$\begin{bmatrix} e_l \\ e_t \\ e_{lt} \end{bmatrix} = \begin{bmatrix} c^2 & s^2 & sc \\ s^2 & c^2 & -sc \\ -2sc & 2sc & c^2 - s^2 \end{bmatrix} \begin{bmatrix} e_x \\ e_q \\ e_{xq} \end{bmatrix} \tag{2}$$

where c = cos (ϕ), s = sin (ϕ) and ϕ is the stiffener orientation angle.

In accordance to assumption (1), the effects of the transverse strain e_t, and the shear strain e_{lt} are neglected. The longitudinal strain e_l expression given below by Equation (3) is obtained from the transformation relation given by Equation (2).

$$e_l = c^2 e_x + s^2 e_q + sc e_{xq} \tag{3}$$

The appropriate angle is substituted in Equation (3) to obtain the strains along all the stiffener directions. In the case of an isogrid stiffener arrangement these angles correspond to 0^o, 60^o, -60^o.

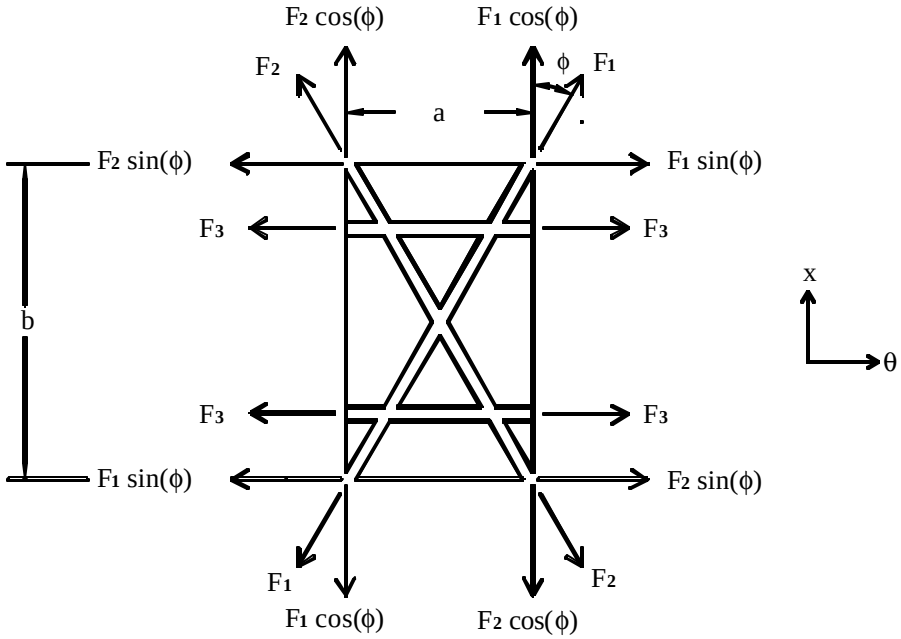

Figure 2. Force diagram.

Once the axial strains on the stiffeners are found, the corresponding axial forces namely F_1, F_2, F_3 are calculated from the longitudinal strains, cross sectional area and longitudinal modulus (E_l) of the stiffeners. Refer to Figure 2 for the force free body diagram of the unit cell.

Equation (4) below shows the resulting three forces.

$$F_1 = AE_l e_{l1} = AE_l(c^2 e_x + s^2 e_q - sce_{xq})$$

$$F_2 = AE_l e_{l2} = AE_l(c^2 e_x + s^2 e_q + sce_{xq}) \quad (4)$$

$$F_3 = AE_l e_{l3} = AE_l(e_q)$$

The resultant forces on each sides of the unit cell are computed by vectorially adding the forces on the stiffeners. Summing up the x-direction forces on either the top or bottom side of the unit cell results in Equation (5).

$$F_x = F_1 \cos(\phi) + F_2 \cos(\phi) \quad (5)$$

Similarly summing up the hoop direction forces on either the left or right side of the unit cell results in Equation (6).

$$F_\theta = F_1 \sin(\phi) + F_2 \sin(\phi) + 2F_3 \quad (6)$$

Expression for the shear force ($F_{x\theta}$), is obtained by adding the force components along any of the sides of the unit cell. Performing this on one of the vertical sides yields Equation (7).

$$F_{x\theta} = F_2 \cos(\phi) - F_1 \cos(\phi) \quad (7)$$

The same shear force expression will result even if the horizontal face is used instead of the vertical face because of the geometrical relations between ‘a’, ‘b’, cos (ϕ), and sin (ϕ).

Substituting Equation (4) into Equations (5), (6), (7):

$$F_x = AE_l c(c^2 e_x + s^2 e_q - sce_{xq}) + AE_l c(c^2 e_x + s^2 e_q + sce_{xq})$$

$$= AE_l (2c^3 e_x + 2s^2 ce_q)$$

$$F_\theta = AE_l s(c^2 e_x + s^2 e_q - sce_{xq}) + AE_l s(c^2 e_x + s^2 e_q + sce_{xq}) + AE_l (e_q)$$

$$= AE_l (sc^2 e_x + (2s^3 + 2)e_q) \quad (8)$$

$$F_{x\theta} = AE_l c(c^2 e_x + s^2 e_q + sce_{xq}) - AE_l c(c^2 e_x + s^2 e_q - sce_{xq})$$

$$= AE_l (2sc^2 e_{xq})$$

The resultant forces, i.e. the forces per unit length N_x, N_θ, and $N_{\theta x}$, are obtained by dividing the above force expressions by the corresponding edge width of the unit cell. After performing this and substituting for the strain terms from Equation (1), expressions for the resultant forces on the unit cell are obtained.

$$N_x = \frac{AE_l}{a}\left[2c^3 e_x^o + 2c^3 k_x(\frac{t}{2}) + 2s^2 ce_q^o + 2s^2 ck_q(\frac{t}{2})\right]$$

$$N_\theta = \frac{AE_l}{b}\left[2sc^2 e_x^o + 2sc^2 k_x(\frac{t}{2}) + (2s^3 + 2)e_q^o + (2s^3 + 2)k_q(\frac{t}{2})\right] \quad (9)$$

$$N_{\theta x} = \frac{AE_l}{b}\left[2sc^2 e_{xq}^o + 2sc^2 k_{xq}(\frac{t}{2})\right]$$

3.2. Moment Analysis

The moments due to the stiffeners is caused by the shear forces on the interface of the shell and the stiffeners. From equilibrium, these shear forces equal to the forces on the stiffeners computed in the previous section. The moment caused by these forces on the mid plane of the shell equals the forces multiplied by one half the shell thickness. The free body diagram in Figure 3(a) shows the different moments created by this force F. Only M_{sh} is of main interest since it is the moment effect of the shear forces on the shell. It can be observed from the free

body diagram a net moment M results on the shell/stiffener assembly. This moment represents the coupling of moment and force resulting from the non-symmetric structure of the shell/stiffener arrangement.

Figure 3(b) shows moment free body diagram of a unit cell. M_1, M_2, and M_3 are the moments resulting from forces F_1, F_2, and F_3 respectively.

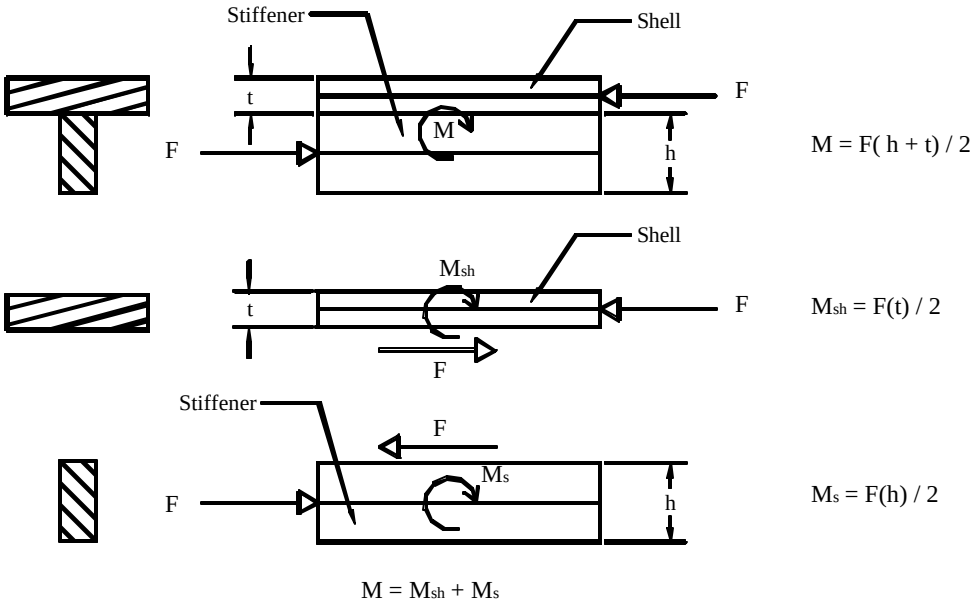

(a) Moments on the skin

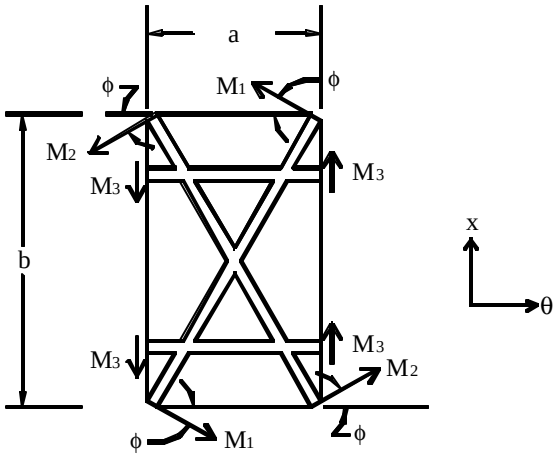

(b) Moments due to stiffeners

Figure 3. Moment diagram.

Following the same procedure as the force analysis on a unit cell, the resultant moments on the horizontal and vertical sides of the unit cell are computed.

$$M_x = M_1 \cos(\phi) + M_2 \cos(\phi) \tag{10a}$$

$$M_\theta = M_1 \sin(\phi) + M_2 \sin(\phi) + 2M_3 \tag{10b}$$

$$M_{x\theta} = M_2 \cos(\phi) - M_1 \sin(\phi) \tag{10c}$$

The moments M_1, M_2, and M_3 are calculated by multiplying the corresponding shear forces (F_1, F_2 and F_3) by the lever arm, which is half the thickness of the shell. Making these substitutions for the moments and dividing by the corresponding edge lengths will result in the resultant moments. Equation (11) shows the final result after simplification.

$$\begin{aligned}
M_x &= \frac{AE_l t}{2a}\left[2c^3 e_x^o + 2c^3 k_x(\frac{t}{2}) + 2s^2 c e_q^o + 2s^2 c k_q(\frac{t}{2})\right] \\
M_\theta &= \frac{AE_l t}{2b}\left[2sc^2 e_x^o + 2sc^2 k_x(\frac{t}{2}) + (2s^3+2) e_q^o + (2s^3+2) k_q(\frac{t}{2})\right] \\
M_{x\theta} &= \frac{AE_l t}{2b}\left[2sc^2 e_{xq}^o + 2sc^2 k_{xq}(\frac{t}{2})\right]
\end{aligned} \tag{11}$$

3.3. The Stiffness Matrix

Equations (9) and (11) are respectively the force and moment contributions of the stiffener, hence hereforth denoted by the superscript ‘s’. These equations are summarized in a matrix form in Equation (12). The resulting matrix elements are functions of the mid plane strains and curvatures of the shell. These were derived by analyzing the force and moments due to stiffeners. We denote these stiffness parameters by $A_{ij}^s, B_{ij}^s, C_{ij}^s$.

$$\begin{bmatrix} N_x^s \\ N_q^s \\ N_{xq}^s \\ M_x^s \\ M_q^s \\ M_{xq}^s \end{bmatrix} = AE_l \begin{bmatrix} \frac{2c^3}{a} & \frac{2s^2c}{a} & 0 & \frac{c^3t}{a} & \frac{s^2ct}{a} & 0 \\ \frac{2sc^2}{b} & \frac{(2s^3+2)}{b} & 0 & \frac{sc^2t}{b} & \frac{(2s^3+2)t}{2b} & 0 \\ 0 & 0 & \frac{2sc^2}{b} & 0 & 0 & \frac{sc^2t}{b} \\ \frac{c^3t}{a} & \frac{s^2ct}{a} & 0 & \frac{c^3t^2}{2a} & \frac{s^2ct^2}{2a} & 0 \\ \frac{sc^2t}{b} & \frac{(2s^3+2)t}{2b} & 0 & \frac{sc^2t^2}{2b} & \frac{(2s^3+2)t^2}{4b} & 0 \\ 0 & 0 & \frac{sc^2t}{b} & 0 & 0 & \frac{sc^2t^2}{2b} \end{bmatrix} \begin{bmatrix} e_x^o \\ e_q^o \\ e_{qx}^o \\ k_x \\ k_q \\ k_{xq} \end{bmatrix} \tag{12}$$

At first glance the stiffness matrix given by Equation (12) might seem unsymmetrical (i.e. $A_{ij} \neq A_{ji} \quad and \quad D_{ij} \neq D_{ji}$), but due to the geometric relation between the parameters 'a', 'b', cos (ϕ) and sin (ϕ) these stiffness quantities can be shown to be equal. It can also be observed the same B_{ij} elements result from the independent force and moment analysis on the unit cell. This is in good agreement with laminate theory, hence further validating the initial assumptions made.

The total force and moment on the panel is the superposition of the force and moment due to the stiffener and the shell. These quantities can be directly superimposed, as the stiffener force and moment contributions have been developed based on the mid plane strains and curvatures. The rule of mixtures is applied and the moments and forces are superimposed according to the volume fractions of the stiffeners and the shell (Equation (13)). V_s and V_{sh} stand for volume fraction of stiffener and shell respectively.

$$\begin{bmatrix} N \\ M \end{bmatrix} = \begin{bmatrix} V_s N^s + V_{sh} N^{sh} \\ V_s M^s + V_{sh} M^{sh} \end{bmatrix} \tag{13}$$

In Equation (13) N^{sh} and M^{sh} are the force and moment contribution of the shell respectively. These quantities are easily computed by applying the laminate theory on the shell.

Substituting the force and moment expressions for the stiffener network from Equation (12) and the corresponding expressions for the shell from the laminate theory results in the panel constitutive equation given by Equation (14). In this equation A, B and D represent the extensional, coupling, and bending stiffness coefficients respectively.

$$\begin{bmatrix} N \\ M \end{bmatrix} = \left[\begin{array}{c|c} V_s A^s + V_{sh} A^{sh} & V_s B^s + V_{sh} B^{sh} \\ \hline V_s B^s + V_{sh} B^{sh} & V_s D^s + V_{sh} D^{sh} \end{array}\right] \begin{bmatrix} e^o \\ k \end{bmatrix} \tag{14}$$

The resultant stiffness parameters obtained from Equation (14) are thus the equivalent stiffness parameters of the whole panel.

3.4. Buckling Load Calculation

The Ritz method is used to calculate the buckling load of the cylinder [14]. The total potential energy of the cylinder Π, is the sum of the strain energy U and the work done by the external force V.

The strain energy for an orthotropic cylinder is given by Equation (15) below [14].

$$\begin{aligned} U = \frac{1}{2}\int_0^{2pr}\int_0^{L} & \{A_{11}(\frac{\partial u}{\partial x})^2 + 2A_{12}\frac{\partial u}{\partial x}(\frac{\partial v}{\partial q}+\frac{w}{r}) + A_{22}[\frac{\partial v}{\partial q}(\frac{\partial v}{\partial q}+\frac{w}{r}) + (\frac{w}{r})^2] \\ & + 2[A_{16}\frac{\partial u}{\partial q} + A_{26}(\frac{\partial v}{\partial q}+\frac{w}{r})](\frac{\partial u}{\partial q}+\frac{\partial v}{\partial x}) + A_{66}(\frac{\partial u}{\partial q}+\frac{\partial v}{\partial x})^2 - B_{11}\frac{\partial u}{\partial x}\frac{\partial^2 w}{\partial x^2} \\ & - 2B_{12}[(\frac{\partial v}{\partial q}+\frac{w}{r})\frac{\partial^2 w}{\partial x^2} + \frac{\partial u}{\partial x}\frac{\partial^2 w}{\partial x^2}] - B_{22}(\frac{\partial v}{\partial q}+\frac{w}{r})\frac{\partial^2 w}{\partial q^2} - 2B_{16}[\frac{\partial^2 w}{\partial x^2}(\frac{\partial u}{\partial q}+\frac{\partial v}{\partial x}) + 2\frac{\partial u}{\partial x}\frac{\partial^2 w}{\partial x \partial q}] \\ & - 2B_{16}[\frac{\partial^2 w}{\partial x^2}(\frac{\partial u}{\partial q}+\frac{\partial v}{\partial x}) + 2\frac{\partial u}{\partial x}\frac{\partial^2 w}{\partial x \partial q}] - 2B_{26}[\frac{\partial^2 w}{\partial q^2}(\frac{\partial u}{\partial q}+\frac{\partial v}{\partial x}) + 2(\frac{\partial v}{\partial q}+\frac{w}{r})\frac{\partial^2 w}{\partial x \partial q}] \\ & - 4B_{66}\frac{\partial^2 w}{\partial x \partial q}(\frac{\partial u}{\partial x}+\frac{\partial v}{\partial q}) + D_{11}(\frac{\partial^2 w}{\partial x^2})^2 + 2D_{12}\frac{\partial^2 w}{\partial x^2}\frac{\partial^2 w}{\partial q^2} + D_{22}(\frac{\partial^2 w}{\partial q^2})^2 \\ & + 4(D_{16}\frac{\partial^2 w}{\partial x^2} + D_{26}\frac{\partial^2 w}{\partial q^2})\frac{\partial^2 w}{\partial x \partial q} + 4D_{66}(\frac{\partial^2 w}{\partial x \partial q})^2\}dx\,dq \end{aligned} \tag{15}$$

This strain energy is a function of the equivalent stiffness parameters of the cylinder panel, the radius of the cylinder ‘r’ and the unknown displacement fields in the radial, axial and hoop

direction ‘w’, ‘u’, and ‘v’ respectively. Since the stiffened cylinder panel has been reduced into an equivalent orthotropic laminate, Equation (15) can be adapted directly.

The potential energy due to in-plane load is in turn given by Equation (16) below. In Equation (16) $N_?$ is the load per unit length applied on the rim of the cylinder.

$$V = \frac{1}{2}\int_0^{2pr}\int_0^{L} N_q \left(\frac{\partial w}{\partial x}\right)^2 dx\,dq \tag{16}$$

The strain energy U and the potential energy term V are integrated along the circumference and the height L of the cylinder to obtain the total energy of the cylinder. The displacement field u, v and w can be defined by kinematically admissible functions, i.e., displacement fields satisfying the essential boundary conditions. Hence they are approximated by a double Fourier series that satisfy the boundary condition requirements. For a simply supported end condition the displacement fields are given by Equation (17) below [16],

$$\begin{aligned} u &= \sum_{m=1}^{\infty}\sum_{n=1}^{\infty} A_{mn} \cos(\bar{m}\,x) \sin(\bar{n}\,s) \\ v &= \sum_{m=1}^{\infty}\sum_{n=1}^{\infty} B_{mn} \sin(\bar{m}\,x) \cos(\bar{n}\,s) \\ w &= \sum_{m=1}^{\infty}\sum_{n=1}^{\infty} C_{mn} \sin(\bar{m}\,x) \sin(\bar{n}\,s) \end{aligned} \tag{17}$$

$\bar{m} = m\pi/L$, $\bar{n} = n/r$, $s = r\theta$, L= height of cylinder and m, n = 1,2,3…

While for a clamped boundary condition the expression for u, v, and w are given by Eqn. (18).

$$\begin{aligned} u &= \sum_{m=1}^{\infty}\sum_{n=1}^{\infty} A_{mn} \cos(\bar{m}\,x) \sin(\bar{n}\,s) \\ v &= \sum_{m=1}^{\infty}\sum_{n=1}^{\infty} B_{mn} \sin(\bar{m}\,x) \cos(\bar{n}\,s) \\ w &= \sum_{m=1}^{\infty}\sum_{n=1}^{\infty} C_{mn} (1-\cos(\bar{m}\,x)) \sin(\bar{n}\,s) \end{aligned} \tag{18}$$

$\bar{m} = m\pi/L$, $\bar{n} = n/r$, $s = r\theta$, and m, n = 1,2,3…

Once the displacement fields are defined, they are substituted into Equations (15) and (16) and integrated between the limits of integration. We sum up the resulting expressions of the strain energy and the work done by the in-plane load and find a general expression for the total energy Π of the system. The total energy expression is a function of the stiffness matrix elements of the equivalent laminate and the unknown displacement field coefficients A_{mn}, B_{mn} and C_{mn}. For the equilibrium to be stable, the total potential energy of the system must be minimum. This can be satisfied by finding the first derivative of the total potential energy with respect to the unknown constants $A_{mn,}$ $B_{mn,}$ and C_{mn} and equating to zero. This results in an eigenvalue problem. The resulting Equation is then solved for the unknown in-plane load $N_?$. A code was developed in Maple to perform all the above tasks (Refer Appendix I). Numerous loads satisfy the expression for in-plane load $N_?$. The minimum value of these loads corresponds to the buckling load of the structure. A Matlab code was developed to calculate the equivalent stiffness parameters of the panel and the minimum buckling load (Refer Appendix II). The code approximates the infinite Fourier series by 100 n and m terms each.

4. FINITE ELEMENTS ANALYSIS

4.1. Modeling

A 3-D model was built for an isogrid stiffened composite cylinder using ANSYS 5.7 finite-elements software (Fig. 4). The modeled cylinder has a radial symmetry of 36^o. Initially one 36^o sector was modeled and then the whole structure was generated using this primary sector.

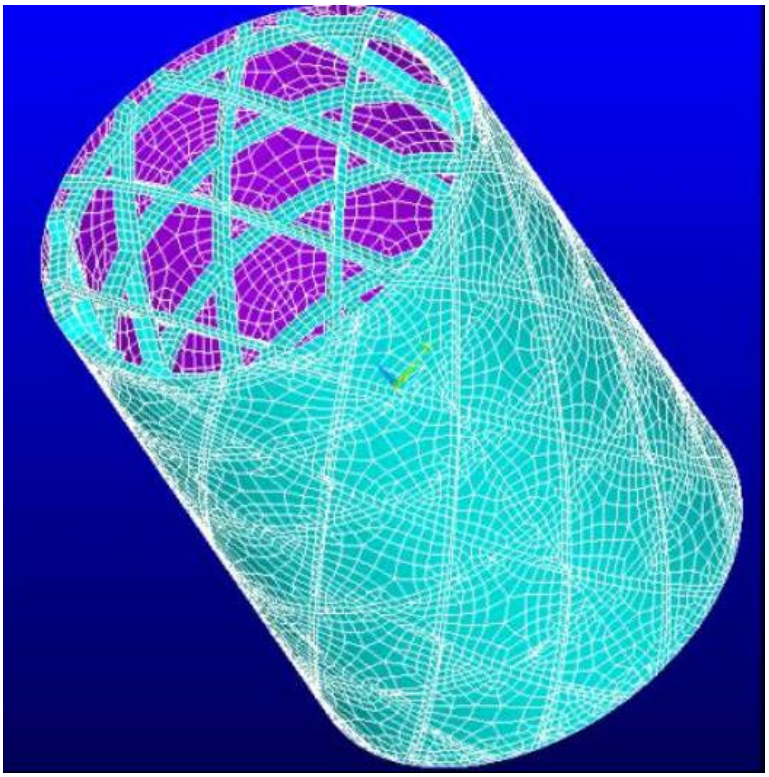

Figure 4. Finite-elements model.

The grid structure was first developed for the primary sector and then the shell was added onto these stiffeners. The $\pm 60^o$ stiffeners in the primary sector were modeled by generating helical rods having outer diameter equal to the inner diameter of the shell. The crossing over points of the stiffeners were modeled by matching the displacement of the corresponding

stiffeners at these points. This was accomplished by merging the nodes of the crossing over stiffeners at the crossover points.

The fibers in the stiffeners are oriented along the length of the stiffeners. Hence, three different real constant tables were defined for the three stiffener orientations of 0^o, 60^o, and -60^o. A local cylindrical coordinate system was then defined for each element and corresponding orthotripic properties aligned properly. The stiffeners were modeled using 20-node, layered solid elements (SOLID 191).

The complete stiffened cylinder under discussion is manufactured by a filament winding process. The skin is made from alternating, numerous $\pm 30^o$ windings. Hence the skin was modeled by a four ply laminate having a stacking sequence of $[30/-30]_s$. Four layers were found to be adequate to model the numerous layers from preliminary buckling analyses done on unstiffened cylindrical shells having different symmetric $\pm 30^o$ plies. The shell and stiffeners were 'glued' at the interface, which upon meshing automatically merges the nodes of the shell elements and the solid element on the interface area. The shell was modeled using 8-node, layered shell element (SHELL 99).

4.2. Meshing

The shell was meshed using quadrilateral shaped elements while the stiffeners were meshed using Hexahedron shaped elements. All the elements have mid nodes. The mesh size used is 4 mm on both shell and stiffeners. This degree of mesh size refinement was chosen based on convergence calculations carried out (refer Section 4.5 for details). This meshing scheme results in approximately 15,000 elements and 250,000 active degrees of freedom (Fig. 4).

4.3. Boundary Conditions and Loading

The global coordinate system of the cylinder is defined in such a way that the bottom face of the cylinder lies in the x-y plane and the positive z-axis is aligned with the axis of the cylinder. The following boundary conditions where imposed on the cylinder.

1. The circumferential and radial displacements 'v' and 'w' respectively equal to zero at both faces of the cylinder (at z=0 and z=h, v=w=0).
2. Axial displacement 'u' is zero at the bottom face of the cylinder but is non-zero at the top face where the load is applied (at z=0, u=0 and at z=h, u≠0).

A uniform unit pressure was applied on the upper rim of the cylinder (z=h). To calculate the buckling load, this unit pressure was multiplied by the area on which the pressure was applied and by the eigenvalue obtained from buckling analysis.

4.4. Solution

Linear buckling analysis in ANSYS finite-elements software is performed in two steps. In the first step a static solution to the structure is obtained. In this analysis the prebuckling stress of the structure is calculated. The second step involves solving the eigenvalue problem given in the form of Equation (19) [12]. This equation takes into consideration the prebuckling stress effect matrix [S] calculated in the first step.

$$([K] + \lambda_i [S])\{y\}_i = \{0\} \tag{19}$$

where [K] = stiffness matrix

[S] = stress stiffness matrix

λ_i = ith eigenvalue (used to multiply the loads which generated [S])

y_i = ith eigenvector of displacements

The 'Block Lanczos' method was used to extract the eigenvalues resulting from Equation (19). The eignevalues obtained from the buckling analysis are factors by which the initially applied unit force is multiplied. As a result, the critical buckling load is calculated according to Equation (20) below.

$$P_{cr} = (l_i)_{\min} AP \tag{20}$$

where $(l_i)_{\min}$ = the minimum eigenvalue

A = total area on which pressure is applied

P = Initially applied pressure

4.5. Convergence

Convergence of the buckling analysis was checked to validate the results obtained from the finite-elements analysis. The convergence check was performed on a model having 75^o stiffeners. The buckling load analysis for this model was done for fine mesh (3 mm), medium mesh (4 mm) and coarse mesh (5 mm). The corresponding buckling loads resulting from these analyses are denoted by L_F, L_M, and L_C. These loads where substituted into the convergence criterion given by Equation (21) below.

$$\left|L_C - L_M\right| > \left|L_C - L_F\right| \tag{21}$$

The convergence check calculation has been summarized in Table 1. From the last column of Table 1, it can be concluded that the analysis has converged for the model developed.

Table 1. Convergence calculation.

L_C	L_M	L_F	$\left\|L_C - L_M\right\|$	$\left\|L_C - L_F\right\|$	$\left\|L_C - L_M\right\| > \left\|L_C - L_F\right\|$
495,000 N	628,357 N	621,598 N	133,357 N	6,759 N	YES (Converges)

It can also be observed that the buckling loads obtained for the medium and coarse mesh schemes (3 mm and 4 mm) are very close to each other, hence a mesh size of 4 mm can be used with out considerable loss of accuracy. Based on this conclusion a mesh size of 4 mm was adopted for all models built.

4.6. Analyses Result

Finite-elements analysis was performed for an isogrid stiffened composite cylinder having the properties shown in Table 2. To study the three buckling failure modes, different analyses were run by varying the skin thickness of the shell while maintaining the same configuration of stiffeners. The skin thickness was varied from 0.3 mm to 4 mm. The observations made on these analyses are presented in the following section.

Table 2. Physical property of model.

Composite System	IM7/977-2
Cylinder height	180 mm
Cylinder diameter	146 mm
Shell winding angle	$\pm 30^{o}$
Stiffeners orientation	0^{o}, $+60^{o}$, -60^{o}
Horizontal stiffener spacing	38.5 mm
Cross stiffeners spacing	42.5 mm
Shell thickness	0.3 mm
Stiffener cross section	6x2.8 mm^2

4.6.1 FAILURE MODES

The cylinder with the thinnest shell thickness of 0.3 mm was observed to fail purely due to local skin buckling (Fig. 5). When the skin thickness was increased, the failure mode gradually changed to global buckling at about 1.5 mm skin thickness. At this point in addition to local buckling of the skin, the adjacent stiffeners started to buckle as well. With further skin thickening of the shell, the localized skin and stiffener failure spread to adjacent cells and gradually transformed to a more global buckling failure mode (Fig. 6). At about a skin thickness of 3 mm, the shell was observed to be relatively stronger than the stiffeners and hence localized stiffener crippling started to occur. For any skin thickness more than 3 mm the local stiffener crippling failure mode prevailed (Fig. 7). It should be noted that the global buckling failure mode observed is not fully developed as would result from a monocoque (unstiffened) cylinder. The failure is hence somewhat localized to a certain portion of the cylinder. It is also observed that there is no unique point at which the failure modes abruptly switch over to the next buckling failure mode but rather go through some transitional mixed buckling failure modes.

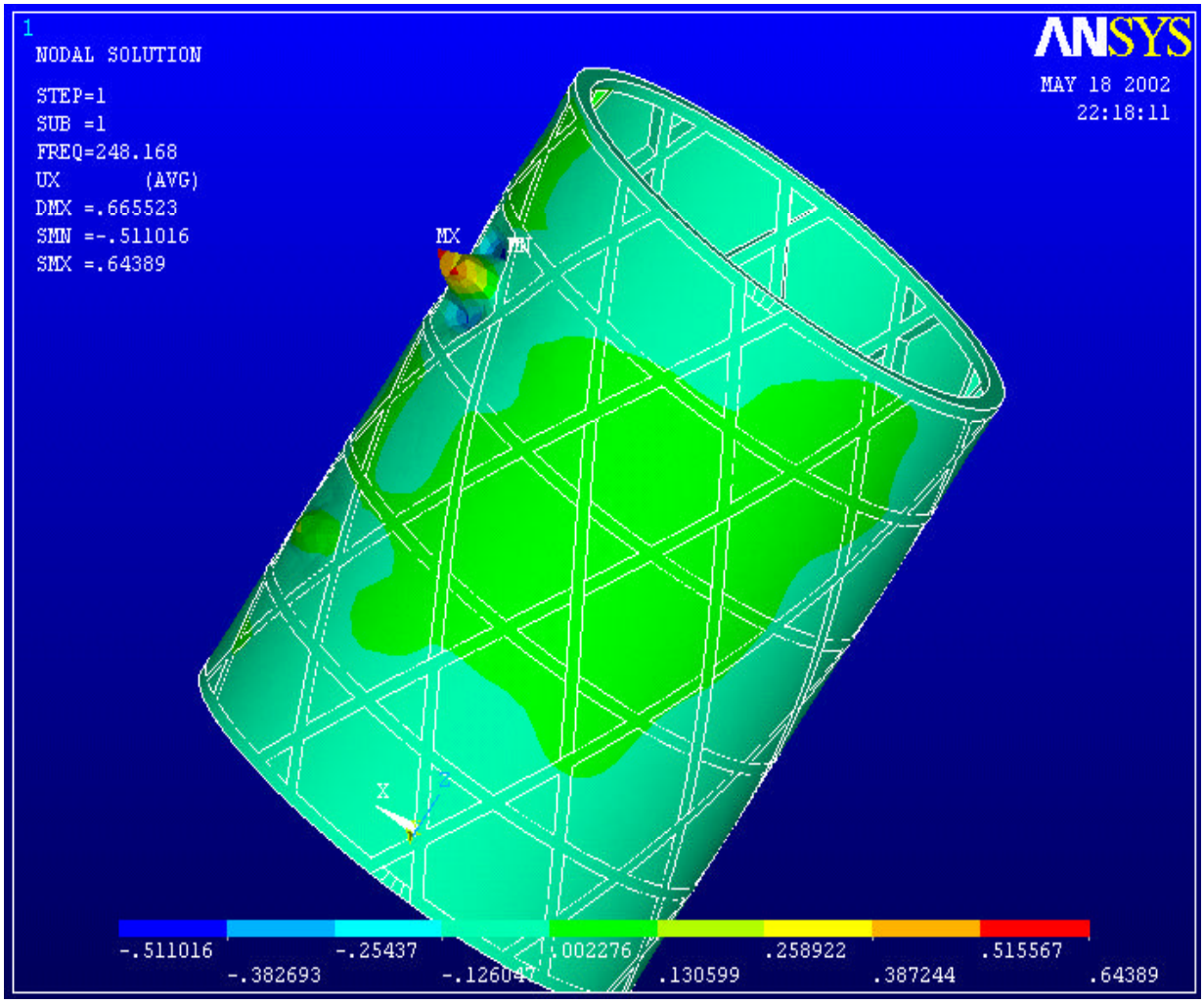

Figure 5. Local skin buckling.

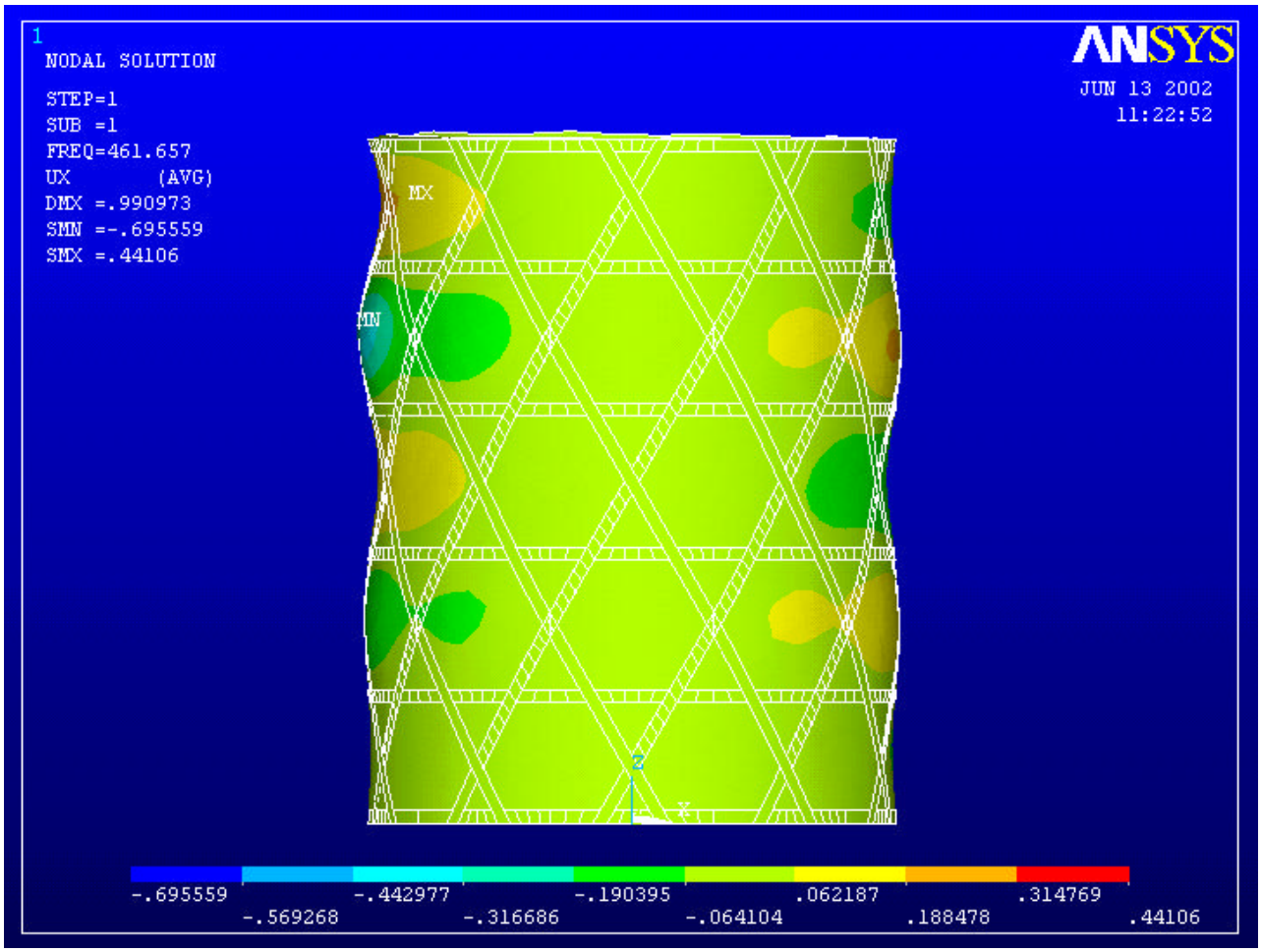

Figure 6. Global buckling.

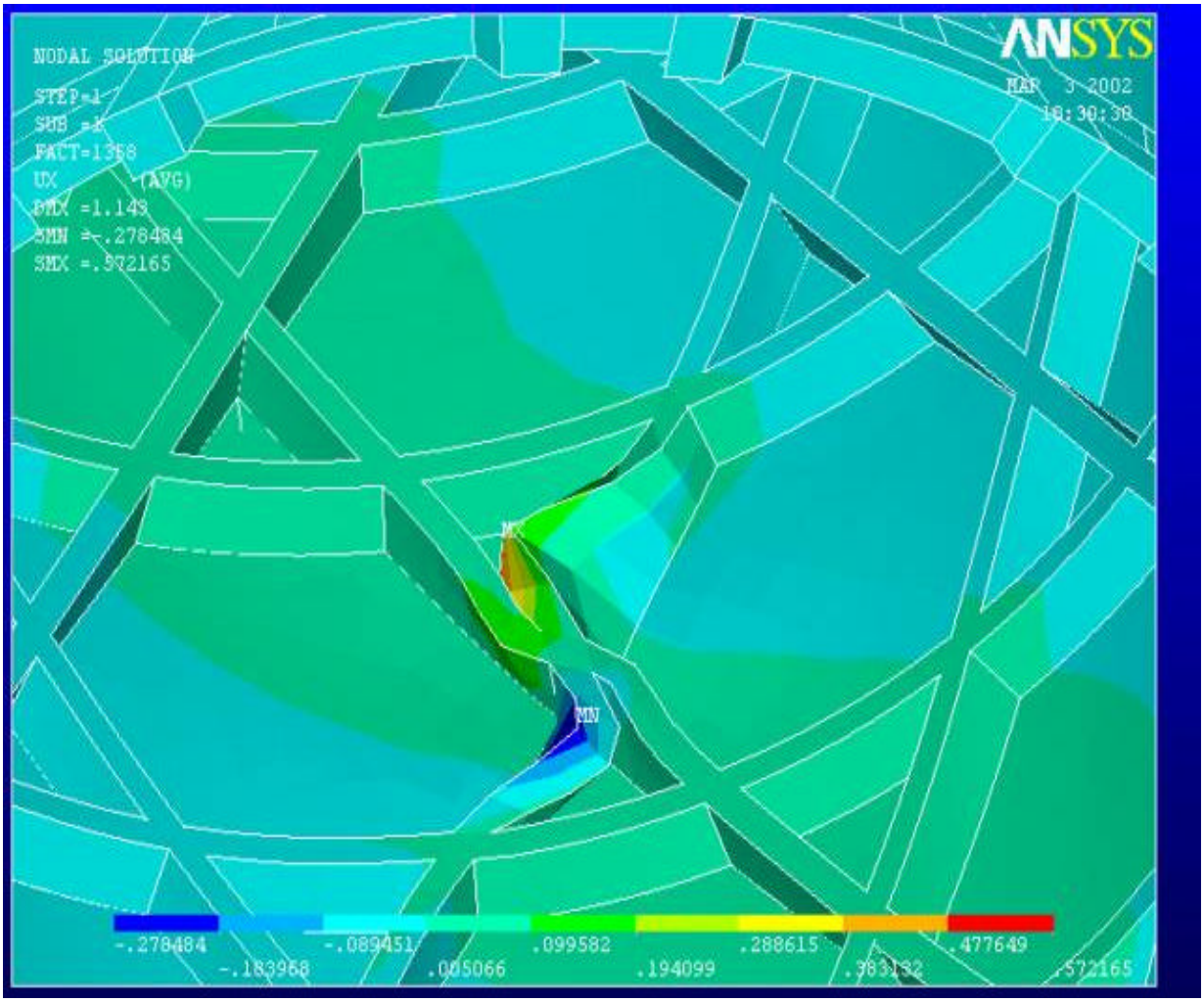

Figure 7. Stiffener crippling.

5. EXPERIMENTATION

In the previous two chapters, two models were developed for buckling investigation of grid-stiffened composite cylinder structures. In order to measure the accuracy of these models, experimental verification is required.

5.1. Test Specimen

The buckling test was performed on an isogrid stiffened composite cylinder. Both the shell and the stiffener of the specimen were integrally made by filament winding process. To avoid material build up at the nodes, the horizontal stiffeners are positioned offset from the intersection point of the cross stiffeners. Figure 8 shows a picture of the specimen.

Figure 8. Test specimen: isogrid stiffened composite cylinder.

The mechanical properties and other significant parameters of the tested specimen are presented in Table 2.

5.2. Test Setup

The test was carried out on an Instron MTS machine. The specimen was placed between two rigid steel plates, with cushioning material between the plate and the cylinder. The cushioning material was used to avoid premature crushing of the cylinder rims. It should be noted that even though the sample was simply supported, the transverse frictional force between the plates and the cylinder couldn't be avoided. The introduction of the cushioning material further increased the transverse friction. Hence the end conditions simulated in the experiment are considered to be somewhere between the clamped and simply supported end conditions. The test set up used is shown in Figure 9 below.

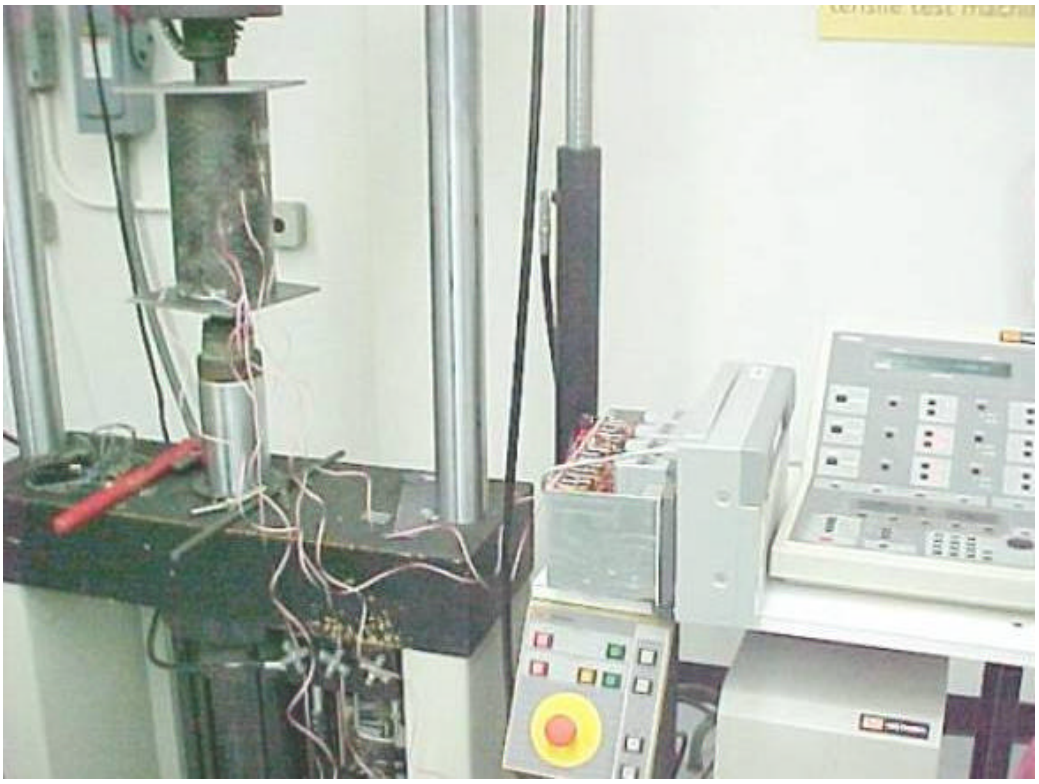

Figure 9. Test set up.

Strains were measured at two locations on the outer surface of the shell. The first strain gauge was fixed at mid height of cylinder while the second was placed near the rim of the cylinder. A

separate unit, YOKOGAWA DC100 data collector, was used to record the strains. Strain measurements were taken every 0.5 seconds and finally saved on a floppy disk as ASCII file by the data collector.

The test was conducted in a displacement-controlled mode with loading rate of 0.26 mm per second. The applied load measurements were saved on a personal computer which is linked to the MTS machine through a data acquisition card. Results obtained for both the strains and load have been plotted with respect to time in Figure 10.

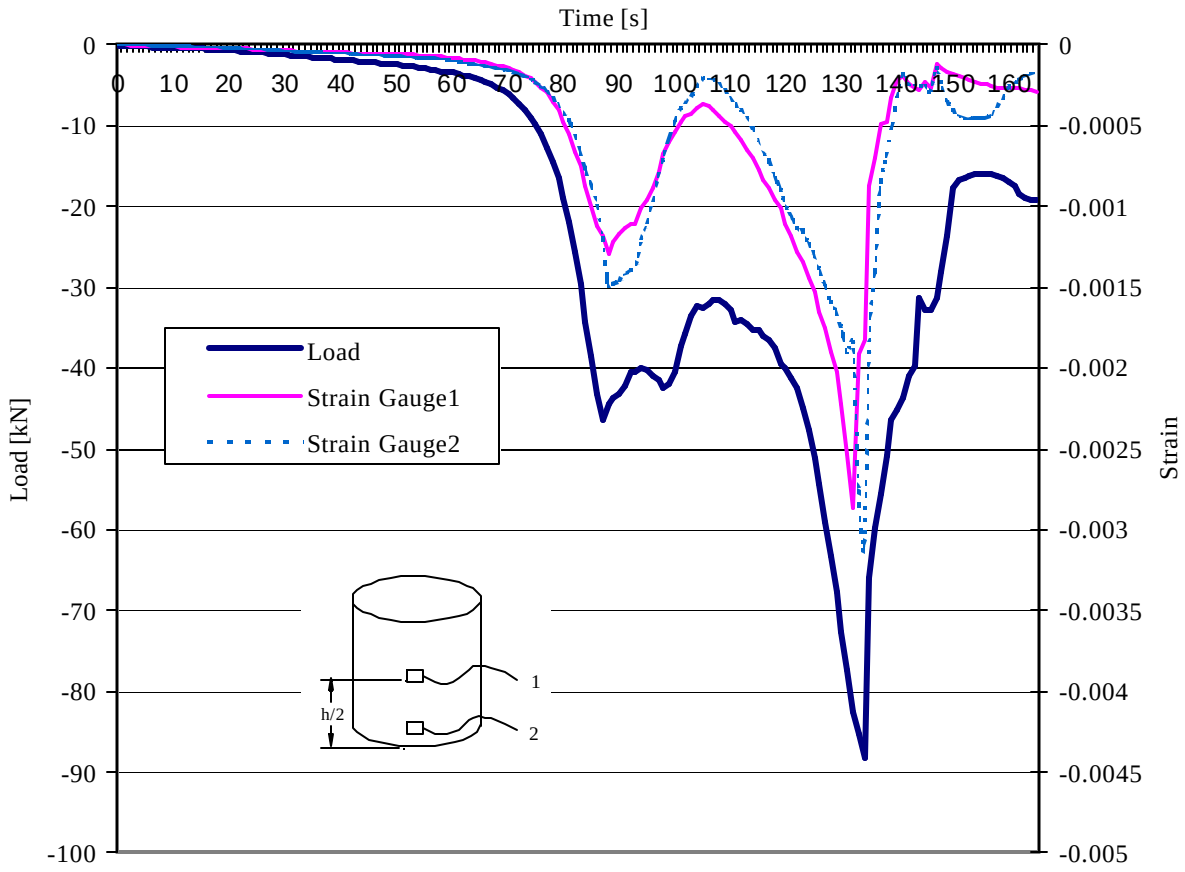

Figure 10. Experimental results.

5.3. Test Result

The result plot in Figure 10 shows two sharp peaks in the load and the strain measurements. The first peak which occurred at 46.7 kN was observed to be a localized failure

of the skin around the lower rim of the cylinder. This is analogous to the local skin buckling failure mode described in the introduction part of this paper. The specimen was further loaded and a drop in the load was observed. This drop of load occurs due to stress redistribution after the local failure occurs. With further loading of the stiffened cylinder, the load gradually increased and reached the second peak at about 88 kN. At this point the specimen failed in global buckling failure mode, and the load dropped sharply. Figure 11 shows pictures of specimen after this global failure.

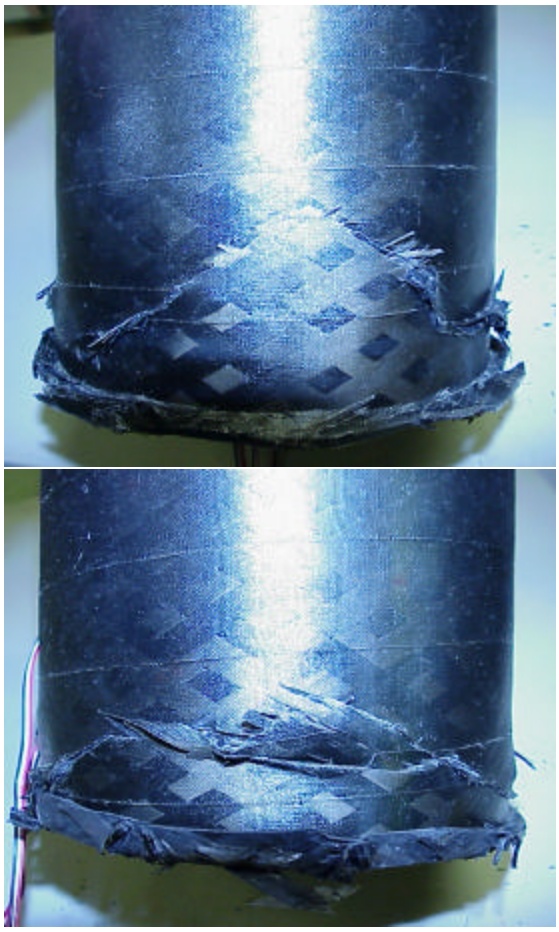

Figure 11. Specimen after failure.

6. RESULTS AND DISCUSSION

In this Chapter comparison of the three different approaches used to calculate buckling load is presented. The comparison is based on analysis performed on the specimen having the properties given in Table 2. These dimensions and configurations were chosen based on the stiffened composite specimen used for experimentation. Since comparison of all three methods at the same time can be confusing, first the experimental result is compared with the results obtained using the smeared model and the finite-elements model. Then the smeared model and finite-elements model are compared.

6.1. Experimental vs. Analytical Models Result Comparison

In chapter five, the failure mode of the specimen was established to be in local skin buckling failure mode. The analytical model developed using smeared approach can only predict global failure modes of a stiffened composite cylinder. Hence, direct comparison of results between the smeared model solution and experimentation is not possible.

On the other hand the finite-elements model built was shown to predict all three types of failure modes of the stiffened composite cylinder. The result of the finite-elements analysis performed on the model built for the specimen showed that the specimen fails in local skin buckling failure mode at a load of 44.9 kN. Figure 5 depicts the failure mode of the specimen from the finite-elements analysis. The finite-element result obtained is within 2.5% deviation from the experimentally found load of 46 kN. Considering the errors that can result from discritization and other sources, we can say the finite-elements analysis accurately models the specimen.

6.2. Smeared Model vs. Finite-elements Model Result Comparison

In Section 6.1 the finite-elements model was verified using experimental results. In this section accuracy of the smeared model is gauged by comparing its results with that of the verified finite-elements model.

The smeared analytical model reduces the whole stiffener/shell panel to an equivalent laminate. The buckling load computed hence assumes a global buckling failure mode. The buckling modes resulting from the smeared model are fully developed lobes both in the hoop and axial direction, since continuous displacement fields were assume.

The buckling load variation with the skin thickness for both finite-element analysis and smeared model is presented in Figure 12. The results for both models are based on calculations made on simply supported models. All parameters are kept the same for both the smeared model and the finite-element model, with cross stiffeners oriented at $\pm 60^{o}$. The error plot (the deviation of smeared model results compared to results obtained using finite-elements analysis) shows that the two analytical models predict almost the same values of buckling load in the global buckling failure mode range. While in the two local failure regions, the smeared model predicts different buckling loads compared to the finite-elements model. This occurs because the equivalent orthotropic cylindrical shell developed using the smeared method will only fail in global buckling failure mode as opposed to the distinct three buckling failure modes occurring in the actual stiffened cylindrical structure. These observations show that the smeared model predicts global buckling failures precisely and confirms that the smeared model cannot be used to analyze local failures.

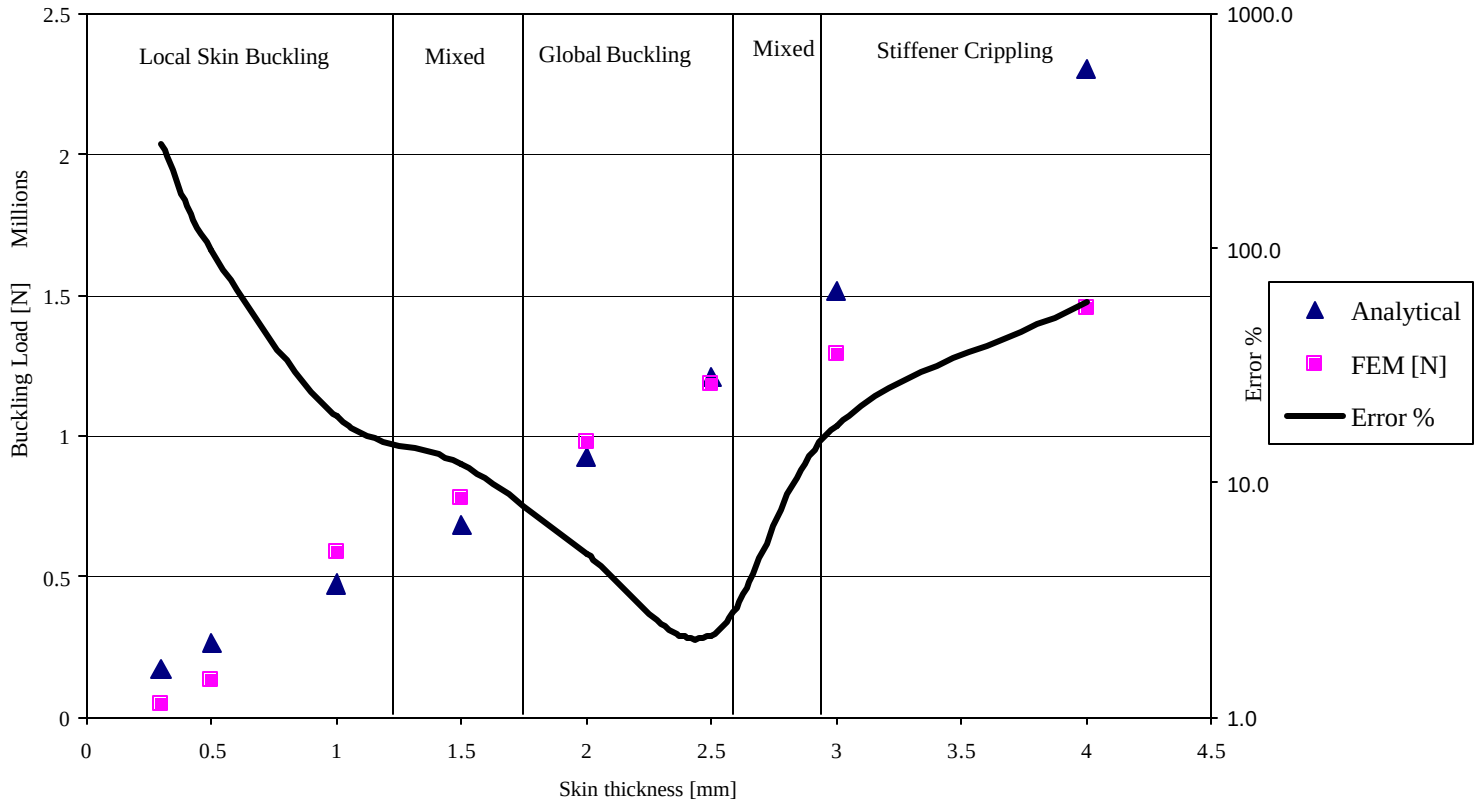

Figure 12. Analytical vs. finite-elements result comparison.

7. PARAMETRIC STUDY

In chapter six the accuracy of the finite-elements model was first verified using experimental results. Then the finite-elements results were used as a benchmark to verify the accuracy of the smeared model developed. Once the accuracy of the smeared model and the finite-elements model was established, parametric study was performed on the different design variables. In this Chapter the effect of shell thickness, shell winding angle, longitudinal modulus and stiffeners orientation angle on buckling load is presented.

Caution should be taken whenever using the smeared analytical model for optimization purposes. This method is exclusively developed for prediction of global failure modes. On the other hand when certain design parameters are varied the failure modes tend to switch over from one kind to another. A good example is the effect of skin thickness. As the skin thickness is increased the failure mode of the stiffened cylinder was shown to change from local skin buckling to global buckling and then to stiffener crippling. Hence, the smeared model cannot be used in this case. In order to use the smeared model without the limitations described, it needs to be used in conjunction with other analytical tools that are able to predict the local failure modes. For the above-mentioned reasons, most of the parametric study is carried out using the finite-elements model.

7.1. Effect of Shell Thickness

The effect of shell thickness on buckling load was investigated using the finite-elements model. Eight analyses were performed to smoothly increase the skin thickness from 0.3 mm to 4 mm. Figure 13 shows plot of the results obtained from these analyses.

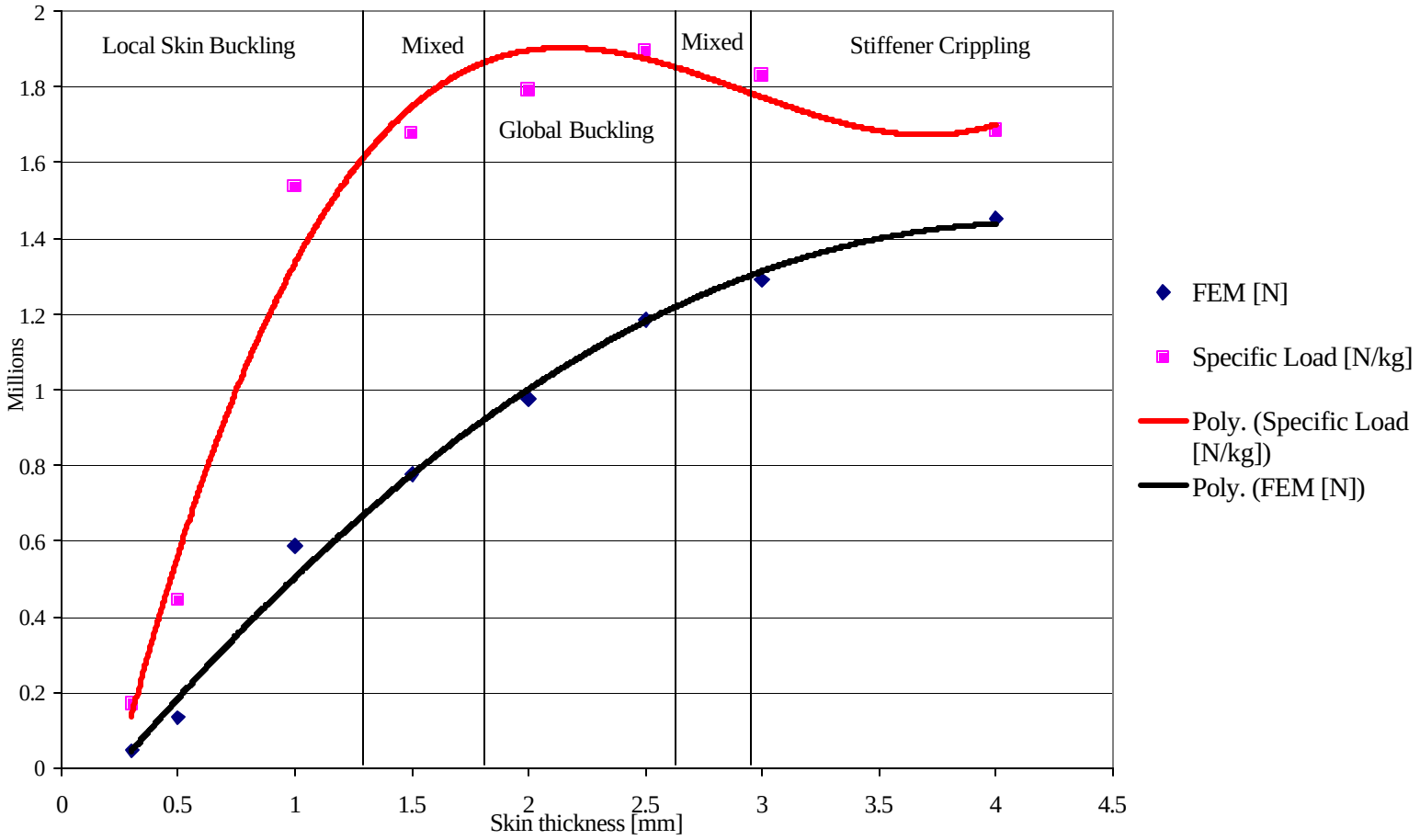

Figure 13. Effect of skin thickness.

It is observed that the buckling resistance of the stiffened cylinder steadily increases with increase in shell thickness. Even though a steady increase in buckling load is observed with skin thickness increase, the gain per unit weight added reaches a maximum and then declines after a certain point. This gain per unit weight, hereforth referred to as 'specific load', measures the efficiency of the weight added, i.e., the additional load carried by the added weight. For the analysis performed on the isogrid stiffener arrangement the optimum skin thickness at which the specific load reaches maximum is found to be 2.2 mm. It can be observed from Figure 13 that this optimum skin thickness lies approximately in the middle of the global buckling failure mode region. This result is very significant as it confirms the observation of other researches [2] that only global buckling failure mode results in the maximum specific buckling load, and consequently leads to the conclusion that global buckling failure mode should be the design criteria for a stiffened cylinder.

7.2. Effect of Shell Winding Angle

Shell winding angle is one of the design variables that can be easily varied using the finite-elements model. The shell winding angle can be varied by just changing the inputs of the real constants table, without changing the model. The effect of shell winding angle was investigated for the three types of buckling failure modes. The analysis was performed on models having skin thickness of 0.3 mm, 2.5 mm and 4 mm. These three skin thickness correspond to local skin buckling, global buckling and stiffener crippling failure modes respectively. The analyses results are presented in Figure 14 below.

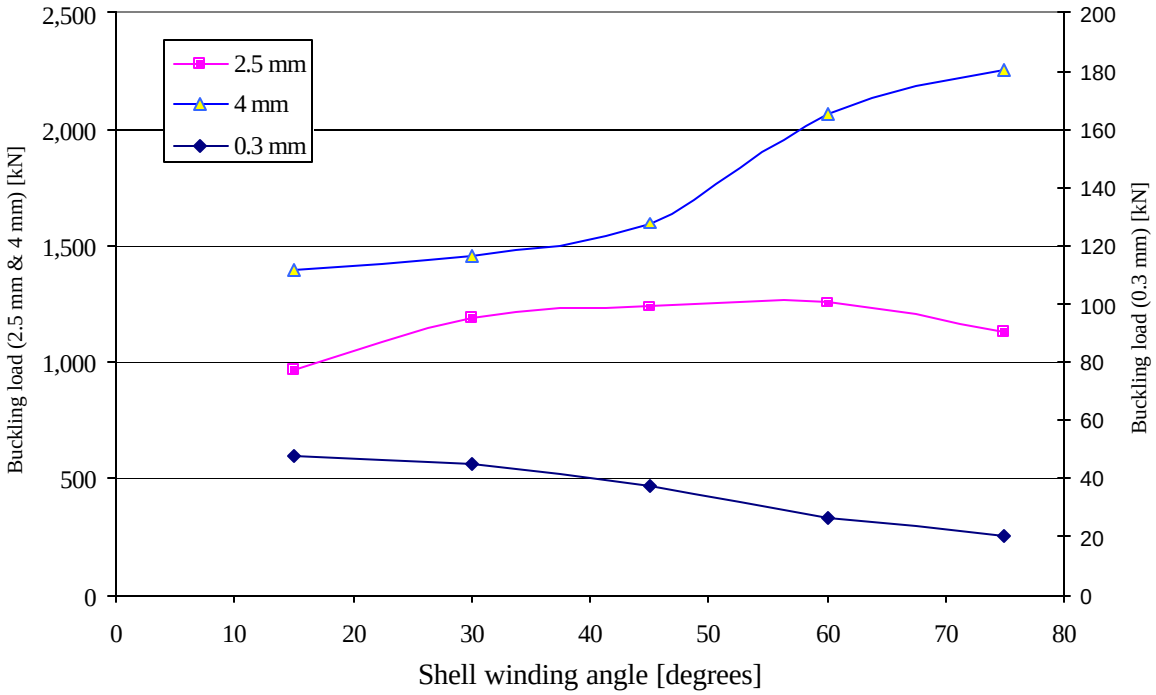

Figure 14. Effect of shell winding angle.

It can be observed that shell winding angle variation has different effects on each type of failure modes. For local skin buckling failure mode, which corresponds to 0.3 mm skin thickness curve, increase in shell winding angle decreases the load resistance of the structure. The effect of shell winding angle on a stiffened cylinder failing in stiffener crippling failure mode is contrary to this. The buckling load resistance increases steadily with winding angle increment. On the other hand, for global buckling failure mode, with increase in shell winding angle the load resistance of the structure first increases and then goes down after reaching a maximum. Hence we can conclude there exists an optimum shell winding angle for a stiffened cylinder failing in global buckling failure mode. The optimum shell winding angle for a stiffened cylinder having a skin thickness of 2.5 mm is found to be about 54^{o}.

7.3. Effect of Stiffener Orientation

The effect of the stiffener orientation was also studied using the finite element model. Four models having cross stiffener orientation angle of 30^o, 45^o, 60^o and 75^o were built for this purpose. The hoop direction is taken as a reference for stiffener orientation angle measurement. In all the four models the total weight of the stiffened cylinder was maintained the same. The result obtained has been summarized in Figure 15 below.

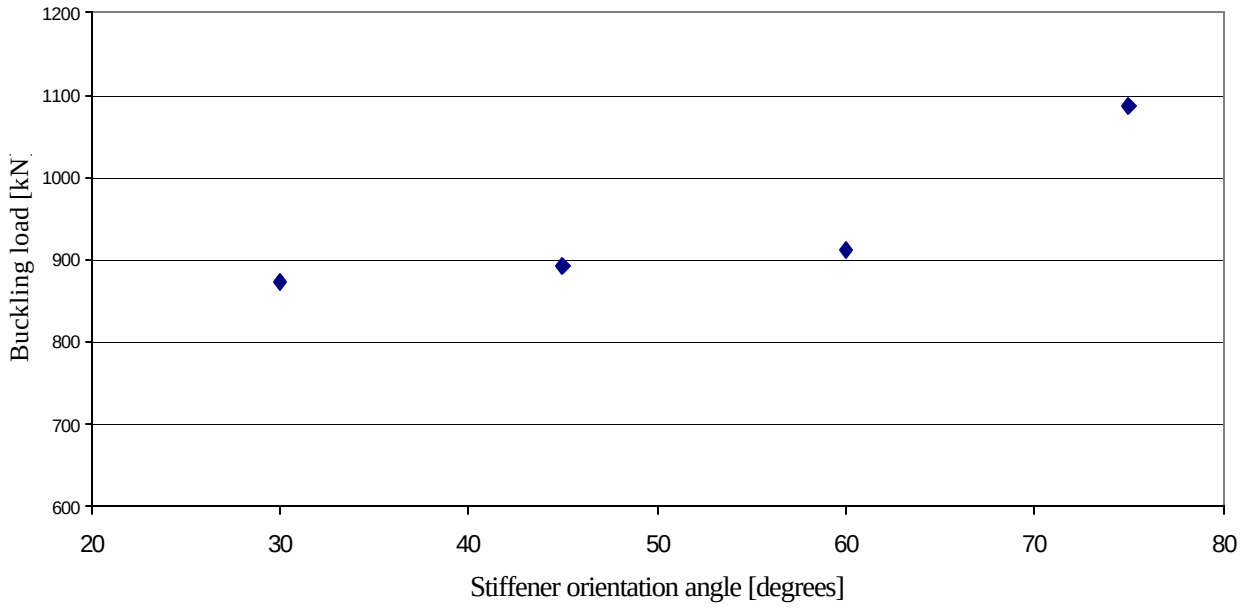

Figure 15. Effect of stiffener orientation.

It can be observed that the buckling resistance of the stiffened cylinder increases when the stiffeners orientation angle is increased. This is reasonable since the applied load is uniaxial and the structure gets stiffer in the axial direction when the stiffener orientation angle is increased.

7.4. Effect of Modulus

The main advantage of developing a closed form analytical solution like the one obtained using the smeared model is the ease with which parametric study can be performed. To demonstrate this advantage, the effect of modulus on the buckling load of an isogrid stiffened composite cylinder was investigated using the smeared model developed. The analysis was

performed for a wide range of skin thickness. It has been shown in Section 7.1 that buckling failure mode highly depends on the skin thickness. As a result the actual failure modes associated with some of the models analyzed might be different from global buckling failure mode. Hence this parametric analysis should only be used to appreciate the use of the smeared analytical model developed and to have a general idea of the effect of modulus on buckling load.

The longitudinal modulus of the composite system was varied from 145Gpa to 192Gpa. The effect of modulus was studied on cylinders having shell thickness varying from 0.3 mm to 4 mm. Figure 16 below summarizes the results obtained.

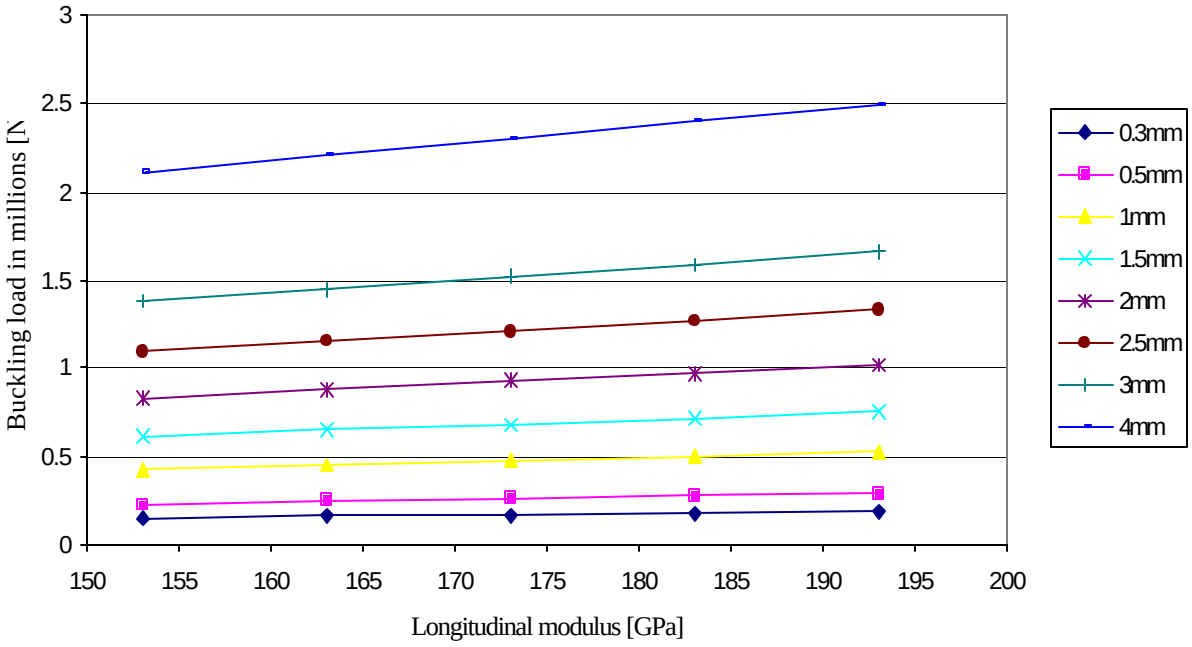

Figure 16. Effect of modulus.

The buckling load was observed to increases linearly with increase in longitudinal modulus for all skin thickness. It appears from the plot that the gain in buckling resistance increases as the skin thickness increases. But a close look at Table 3, which tabulates the percentage gain in the buckling load with increase in modulus, shows a higher gain in buckling load is obtained for lower skin thickness.

Table 3. Gain in buckling load with modulus increase.

Skin thickness	0.3 mm	0.5 mm	1 mm	1.5 mm	2 mm	2.5 mm	3 mm	4 mm
% Load gain	26.0	25.7	24.9	23.8	22.1	21.8	20.2	17.7

Hence it can be concluded that a better gain in buckling load resistance is achieved if the longitudinal modulus is increased for a stiffened cylinder failing in local skin buckling failure mode than for a stiffened cylinder failing in a stiffener crippling failure mode.

8. CONCLUSION

A smeared stiffener analytical model was successfully developed for the investigation of buckling problems of stiffened composite cylinders. This analytical model is robust in that it can be used to predict the global buckling loads of composite cylinders stiffened either on one side or both sides. Finite-elements analysis and experimentation were carried out to assess the reliability of this analytical model. Based on comparisons made in Chapter 6, the analytical model developed has been found to be very accurate in predicting the global failure loads of stiffened composite cylinders.

The different failure modes of a stiffened composite cylinder were also studied in detail. These studies showed that the efficient utilization of material (load resistance per unit weight) highly depends on the buckling failure mode of the cylinder structure. For an isogrid stiffened cylinder, failure in global buckling mode resulted in the highest specific buckling load.

Based on the analytical models developed, parametric study was performed on some of the design variables involved in stiffened composite cylinders. The parameters investigated were skin thickness, skin winding angle, stiffener orientation angle and longitudinal modulus.

Increase in skin thickness was shown to increase the buckling resistance of the stiffened structure continuously. But an optimum skin thickness of 2.2 mm was observed to result in the highest specific buckling load.

The variation in shell winding angle was observed to have different effects on stiffened cylinders failing in different failure modes. For a stiffened cylinder failing in local skin buckling failure mode, increase in winding angle decreases the load resistance of the structure. While for a stiffened cylinder failing in stiffener crippling failure mode, improvement in load resistance is

noted with increase in shell winding angle. For a stiffened cylinder failing in global buckling failure mode an optimum shell-winding angle of 54^{o} was observed.

The effects of both stiffener orientation angle and longitudinal modulus increase were observed to continuously increase the buckling resistance of the stiffened cylinder structure.

REFERENCES

1. Jaunky N., Knight N.F., Ambur D.R., "Optimal Design of General Stiffened Composite Circular Cylinders for Global Buckling With Strength Constraints," Composite Structures, March 1998.

2. Helms J.E., Li G., Smith B.H., "Analysis of Grid Stiffened Cylinders," ASME/ETCE 2001.

3. Black S., "A Grid-Stiffened Alternative to Cored Laminates," High-Performance Composites, March 2002.

4. Jaunky N., Knight N.F., Ambur D.R., "Formulation of An Improved Smeared Stiffener Theory of Buckling Analysis of Grid-Stiffened Composite Panels," NASA technical Memorandum 110162, June 1995.

5. Phillips J.L., Gurdal Z., "Structural Analysis and Optimum Design of Geodesically Stiffened Composite Panels," NASA Report CCMS-90-05, July 1990.

6. Gerdon G., Gurdal Z., "Optimal Design of Geodesically Stiffened Composite Cylindrical Shells," AIAA Journal, November 1985; 23(11): 1753-1761.

7. Jaunky N., Knight N.F., Ambur D.R., "Optimal Design of Grid-Stiffened Composite Panels Using Global and Local Buckling Analysis," Journal of Aircraft, Vol. 35, No. 3, May-June 1998.

8. Wang J.T.S., Hsu T.M., "Discrete Analysis of Stiffened Composite Cylindrical Shells," AIAA J. 1995, 23, 1753-1761.

9. Knight N.F., Stranes J.H., "Development in Cylindrical Shell Stability Analysis," NASA report, 1997.

10. Graham J., "Preliminary Analysis Techniques for Ring and Stringer Stiffened Cylindrical Shells," NASA report TM-108399, March 1993.

11. Hilburger M.W., "Nonlinear and Buckling Behavior of Compression-loaded Composite Shells," Proceedings of the 6th Annual Technical Conference of the American Society for Composites, Virginia 2001.

12. ANSYS THEORY REFERENCE. http://www1.ansys.com/customer/content/documentation/60/ch01.html

13. Hyer M.W., Riddick J.C., "Effect of Imperfections of Buckling and Postbuckling Response of Segmented Circular Composite Cylinders," Proceedings of the 6th Annual Technical Conference of the American Society for Composites, Virginia 2001.

14. Whitney J.M., "Structural Analysis of Laminated Anisotropic Plates," Technomic, 1987.

15. Agarwal B.D., Broutman L.J., “Analysis and Performance of Fiber Composites,” John Wiley and Sons, 1990.

16. Brush D.O., Almroth B.O., “Buckling of Bars, Plates, and Shells,” McGraw-Hill Book Company, New York, NY 1975.

17. Bruhn E.F., “Analysis and Design of Flight Vehicle Structures.” Jacobs Publishing, Inc., Carmel, IN June 1973.

18. Ramm E., “Buckling of Shells,” Springer-Verlag, Berlin 1982.

19. Dow N.F., Libove C., Hubka R.E., “Formulas for Elastic Constants of Plates with Integral Waffle-like Stiffening,” NACA RM L53L1 3a, August 1953.

APPENDICES

A. Maple Code

```
> w:=C*(sin(M*x))*sin(N*s);
```

$$w := C \sin(M x) \sin(N s)$$

```
> u:=A*(cos(M*x))*sin(N*s);
```

$$u := A \cos(M x) \sin(N s)$$

```
> v:=B*(sin(M*x))*cos(N*s);
```

$$v := B \sin(M x) \cos(N s)$$

```
>
U:=A11*(diff(u,x))^2+2*A12*(diff(u,x))*(diff(v,s)+w/r)+A22*(diff
(v,s)*(diff(v,s)+w/r)+(w/r)^2)+A66*(diff(u,s)+diff(v,x))^2-
B11*diff(u,x)*diff(diff(w,x),x)-
2*B12*((diff(v,s)+w/r)*diff(diff(w,x),x)+diff(u,x)*diff(diff(w,s
),s))-B22*(diff(v,s)+w/r)*diff(diff(w,s),s)-
4*B66*diff(diff(w,s),x)*(diff(u,x)+diff(v,s))+D11*(diff(diff(w,x
),x))^2+2*D12*diff(diff(w,x),x)*diff(diff(w,s),s)+D22*(diff(diff
(w,s),s))^2+4*(D16*diff(diff(w,x),x)+D26*diff(diff(w,s),s))*diff
(diff(w,s),x)+4*D66*(diff(diff(w,x),s))^2;
```

$$\begin{aligned}
U := {} & A11\, A^2 \sin(M x)^2 M^2 \sin(N s)^2 \\
& - 2\, A12\, A \sin(M x) M \sin(N s) \left(-B \sin(M x) \sin(N s) N + \frac{C \sin(M x) \sin(N s)}{r} \right) + \\
& A22 \left(-B \sin(M x) \sin(N s) N \left(-B \sin(M x) \sin(N s) N + \frac{C \sin(M x) \sin(N s)}{r} \right) \right. \\
& \left. + \frac{C^2 \sin(M x)^2 \sin(N s)^2}{r^2} \right) \\
& + A66 (A \cos(M x) \cos(N s) N + B \cos(M x) M \cos(N s))^2 \\
& - B11\, A \sin(M x)^2 M^3 \sin(N s)^2 C - 2\, B12 \\
& \left(- \left(-B \sin(M x) \sin(N s) N + \frac{C \sin(M x) \sin(N s)}{r} \right) C \sin(M x) M^2 \sin(N s) \right. \\
& \left. + A \sin(M x)^2 M \sin(N s)^2 C N^2 \right) \\
& + B22 \left(-B \sin(M x) \sin(N s) N + \frac{C \sin(M x) \sin(N s)}{r} \right) C \sin(M x) \sin(N s) N^2 - \\
& 4\, B66\, C \cos(M x) M \cos(N s) N (-A \sin(M x) M \sin(N s) - B \sin(M x) \sin(N s) N) \\
& + \mathrm{D11}\, C^2 \sin(M x)^2 M^4 \sin(N s)^2 + 2\, \mathrm{D12}\, C^2 \sin(M x)^2 M^2 \sin(N s)^2 N^2 \\
& + \mathrm{D22}\, C^2 \sin(M x)^2 \sin(N s)^2 N^4 + 4 \\
& (-\mathrm{D16}\, C \sin(M x) M^2 \sin(N s) - \mathrm{D26}\, C \sin(M x) \sin(N s) N^2)\, C \cos(M x) M \\
& \cos(N s) N + 4\, \mathrm{D66}\, C^2 \cos(M x)^2 M^2 \cos(N s)^2 N^2
\end{aligned}$$

```
> with(student):
>
X:=eval(value(Doubleint(0.5*U,x=0..l,s=0..2*pi*r)),{sin(2.*r*pi*
N)=0,sin(l*M)=0,(cos(l*M))^2=1});
```

$$X := .1250000000\,(2.\,\mathrm{D11}\,C^2 M^5 r^3 l\,\pi N + 2.\,A66\,r^3 l M^3 B^2 \pi N + 2.\,A11\,A^2 M^3 r^3 l\,\pi N - 4.\,B12\,C r^3 M^3 l B N^2 \pi - 2.\,A22\,l M B r^2 C N^2 \pi + 2.\,\mathrm{D22}\,C^2 N^5 r^3 l M \pi + 2.\,A66\,r^3 l M A^2 N^3 \pi + 2.\,A22\,l M B^2 N^3 r^3 \pi + 2.\,B22\,C^2 N^3 r^2 l M \pi + 2.\,A22\,l M C^2 r \pi N - 2.\,B22\,C N^4 r^3 l M B \pi + 8.\,\mathrm{D66}\,C^2 M^3 N^3 r^3 l \pi - 4.\,B12\,C r^3 M^2 l A N^3 \pi + 4.\,\mathrm{D12}\,C^2 M^3 N^3 r^3 l \pi - 2.\,B11\,A M^4 C r^3 l \pi N - 4.\,A12\,A r^2 M^2 l C \pi N + 4.\,B12\,C^2 r^2 M^3 l \pi N + 4.\,A12\,A r^3 M^2 l B N^2 \pi + 4.\,A66\,r^3 l M^2 A B N^2 \pi) / (r^2 M N)$$

```
> V:=-0.5*No*(diff(w,x))^2;
>
```

$$V := -.5\,No\,C^2 \cos(M x)^2 M^2 \sin(N s)^2$$

```
>
VV:=eval(value(Doubleint(V,x=0..l,s=0..2*pi*r)),{sin(l*M)=0,sin(
2.*r*pi*N)=0,(cos(l*M))^2=1});
```

$$VV := -.2500000000\,No\,C^2 M^2 l r \pi$$

```
> TE:=(X+VV);
>
```

$$TE := .1250000000\,(2.\,\mathrm{D11}\,C^2 M^5 r^3 l\,\pi N + 2.\,A66\,r^3 l M^3 B^2 \pi N + 2.\,A11\,A^2 M^3 r^3 l\,\pi N - 4.\,B12\,C r^3 M^3 l B N^2 \pi - 2.\,A22\,l M B r^2 C N^2 \pi + 2.\,\mathrm{D22}\,C^2 N^5 r^3 l M \pi + 2.\,A66\,r^3 l M A^2 N^3 \pi + 2.\,A22\,l M B^2 N^3 r^3 \pi + 2.\,B22\,C^2 N^3 r^2 l M \pi + 2.\,A22\,l M C^2 r \pi N - 2.\,B22\,C N^4 r^3 l M B \pi + 8.\,\mathrm{D66}\,C^2 M^3 N^3 r^3 l \pi - 4.\,B12\,C r^3 M^2 l A N^3 \pi + 4.\,\mathrm{D12}\,C^2 M^3 N^3 r^3 l \pi - 2.\,B11\,A M^4 C r^3 l \pi N - 4.\,A12\,A r^2 M^2 l C \pi N + 4.\,B12\,C^2 r^2 M^3 l \pi N + 4.\,A12\,A r^3 M^2 l B N^2 \pi + 4.\,A66\,r^3 l M^2 A B N^2 \pi) / (r^2 M N) - .2500000000\,No\,C^2 M^2 l r \pi$$

```
> E1:=diff(TE,A)*4/l/pi=0;
```

$$E1 := .5000000000\,(4.\,A11\,A M^3 r^3 l\,\pi N + 4.\,A66\,r^3 l M A N^3 \pi - 4.\,B12\,C r^3 M^2 l N^3 \pi - 2.\,B11\,M^4 C r^3 l\,\pi N - 4.\,A12\,r^2 M^2 l C \pi N + 4.\,A12\,r^3 M^2 l B N^2 \pi + 4.\,A66\,r^3 l M^2 B N^2 \pi) / (r^2 M N l \pi) = 0$$

```
> simplify(%);
```

$$2.\,A11\,A M^2 r + 2.\,A66\,r A N^2 - 2.\,B12\,C r M N^2 - 1.\,B11\,M^3 C r - 2.\,A12\,M C + 2.\,A12\,r M B N + 2.\,A66\,r M B N = 0$$

```
> E2:=diff(TE,B)*4/l/pi=0;
```

$$E2 := .5000000000\,(4.\,A66\,r^3\,l\,M^3\,B\,\pi\,N - 4.\,B12\,C\,r^3\,M^3\,l\,N^2\,\pi - 2.\,A22\,l\,M\,r^2\,C\,N^2\,\pi + 4.\,A22\,l\,M\,B\,N^3\,r^3\,\pi - 2.\,B22\,C\,N^4\,r^3\,l\,M\,\pi + 4.\,A12\,A\,r^3\,M^2\,l\,N^2\,\pi + 4.\,A66\,r^3\,l\,M^2\,A\,N^2\,\pi)\,/\,(r^2\,M\,N\,l\,\pi) = 0$$

```
> simplify(%);
```

$$2.\,A66\,r\,M^2\,B - 2.\,B12\,C\,r\,M^2\,N - 1.\,A22\,C\,N + 2.\,A22\,B\,N^2\,r - 1.\,B22\,C\,N^3\,r + 2.\,A12\,A\,r\,M\,N + 2.\,A66\,r\,M\,A\,N = 0$$

```
> E3:=diff(TE,C)*4/l/pi=0;
```

$$E3 := 4\,(.1250000000\,(4.\,\mathrm{D11}\,C\,M^5\,r^3\,l\,\pi\,N - 4.\,B12\,r^3\,M^3\,l\,B\,N^2\,\pi - 2.\,A22\,l\,M\,B\,r^2\,N^2\,\pi + 4.\,\mathrm{D22}\,C\,N^5\,r^3\,l\,M\,\pi + 4.\,B22\,C\,N^3\,r^2\,l\,M\,\pi + 4.\,A22\,l\,M\,C\,r\,\pi\,N - 2.\,B22\,N^4\,r^3\,l\,M\,B\,\pi + 16.\,\mathrm{D66}\,C\,M^3\,N^3\,r^3\,l\,\pi - 4.\,B12\,r^3\,M^2\,l\,A\,N^3\,\pi + 8.\,\mathrm{D12}\,C\,M^3\,N^3\,r^3\,l\,\pi - 2.\,B11\,A\,M^4\,r^3\,l\,\pi\,N - 4.\,A12\,A\,r^2\,M^2\,l\,\pi\,N + 8.\,B12\,C\,r^2\,M^3\,l\,\pi\,N)\,/\,(r^2\,M\,N) - .5000000000\,No\,C\,M^2\,l\,r\,\pi)/(l\,\pi) = 0$$

```
> simplify(%);
```

$$-1.\,(-2.\,\mathrm{D11}\,C\,M^4\,r^2 + 2.\,B12\,r^2\,M^2\,B\,N + A22\,B\,r\,N - 2.\,\mathrm{D22}\,C\,N^4\,r^2 - 2.\,B22\,C\,N^2\,r - 2.\,A22\,C + B22\,N^3\,r^2\,B - 8.\,\mathrm{D66}\,C\,M^2\,N^2\,r^2 + 2.\,B12\,r^2\,M\,A\,N^2 - 4.\,\mathrm{D12}\,C\,M^2\,N^2\,r^2 + B11\,A\,M^3\,r^2 + 2.\,A12\,A\,r\,M - 4.\,B12\,C\,r\,M^2 + 2.\,No\,C\,M^2\,r^2)/r = 0$$

```
>
> with(linalg):

> DD:=Matrix([[a11,a12,a13],[a12,a22,a23],[a13,a23,a33-
2*No*M^2*r]]);
```

$$DD := \begin{bmatrix} a11 & a12 & a13 \\ a12 & a22 & a23 \\ a13 & a23 & a33 - 2\,No\,M^2\,r \end{bmatrix}$$

```
> FF:=det(DD)=0;
```

$$FF := a11\,a22\,a33 - 2\,a11\,a22\,No\,M^2\,r - a11\,a23^2 - a12^2\,a33 + 2\,a12^2\,No\,M^2\,r + 2\,a12\,a13\,a23 - a13^2\,a22 = 0$$

```
> 2*pi*r*solve(FF,No);
```

$$\frac{\pi\,(a11\,a22\,a33 + 2\,a12\,a13\,a23 - a11\,a23^2 - a12^2\,a33 - a13^2\,a22)}{M^2\,(-a12^2 + a11\,a22)}$$

```
> restart;
```

B. Matlab Code

```
clear all;
teta=[30 -30 60 -60 0]*pi/180;
Q11=173;
Q22=7.63;
Q12=2.289;
Q66=5.5;
a=146.3/2000; %Radius of cylinder%
L=190/1000; %Height of cylinder%
A=(5.25e-3)*(4.1e-3); %cross section area of stiffners%
b=72.62e-3; %Axial pitch%
aa=45.9e-3; %Radial pitch%

Qbar11=Q11*(cos(teta)).^4+Q22*(sin(teta)).^4+2*(Q12+2*Q66)*(sin(teta)).^2.*
(cos(teta)).^2;
Qbar22=Q11*(sin(teta)).^4+Q22*(cos(teta)).^4+2*(Q12+2*Q66)*(sin(teta)).^2.*
(cos(teta)).^2;
Qbar12=(Q11+Q22-*Q66)*((sin(teta)).^2).*((cos(teta)).^2)+Q12*((cos(teta)).^4+
(sin(teta)).^4);
Qbar66=(Q11+Q22-2*Q12-
2*Q66)*(sin(teta)).^2.*(cos(teta)).^2+Q66*((cos(teta)).^4+(sin(teta)).^4);
Qbar16=(Q11-Q12-2*Q66)*(cos(teta)).^3.*sin(teta)-(Q22-Q12-
2*Q66)*cos(teta).*(sin(teta)).^3;
Qbar26=(Q11-Q12-2*Q66)*(cos(teta)).*(sin(teta)).^3-(Q22-Q12-
2*Q66)*(cos(teta)).^3.*(sin(teta));

t=[0.3 0.5 1 1.5 2 2.5 3 4]/1000;

for o=1:8;
ho=-t(o)/2;
h1=ho+t(o)/4;
h2=h1+t(o)/4;
h3=h2+t(o)/4;
h4=h3+t(o)/4;

A11=Qbar11(1)*(h1-ho)+Qbar11(2)*(h2-h1)+Qbar11(2)*(h3-h2)+Qbar11(1)*(h4-h3);
A22=Qbar22(1)*(h1-ho)+Qbar22(2)*(h2-h1)+Qbar22(2)*(h3-h2)+Qbar22(1)*(h4-h3);
A12=Qbar12(1)*(h1-ho)+Qbar12(2)*(h2-h1)+Qbar12(2)*(h3-h2)+Qbar12(1)*(h4-h3);
A16=Qbar16(1)*(h1-ho)+Qbar16(2)*(h2-h1)+Qbar16(2)*(h3-h2)+Qbar16(1)*(h4-h3);
A26=Qbar26(1)*(h1-ho)+Qbar26(2)*(h2-h1)+Qbar26(2)*(h3-h2)+Qbar26(1)*(h4-h3);
A66=Qbar66(1)*(h1-ho)+Qbar66(2)*(h2-h1)+Qbar66(2)*(h3-h2)+Qbar66(1)*(h4-h3);

B11=1/2*(Qbar11(1)*(h1^2-ho^2)+Qbar11(2)*(h2^2-h1^2)+Qbar11(2)*(h3^2-
h2^2)+Qbar11(1)*(h4^2-h3^2));
B22=1/2*(Qbar22(1)*(h1^2-ho^2)+Qbar22(2)*(h2^2-h1^2)+Qbar22(2)*(h3^2-
h2^2)+Qbar22(1)*(h4^2-h3^2));
B12=1/2*(Qbar12(1)*(h1^2-ho^2)+Qbar12(2)*(h2^2-h1^2)+Qbar12(2)*(h3^2-
h2^2)+Qbar12(1)*(h4^2-h3^2));
B16=1/2*(Qbar16(1)*(h1^2-ho^2)+Qbar16(2)*(h2^2-h1^2)+Qbar16(2)*(h3^2-
h2^2)+Qbar16(1)*(h4^2-h3^2));
B26=1/2*(Qbar26(1)*(h1^2-ho^2)+Qbar26(2)*(h2^2-h1^2)+Qbar26(2)*(h3^2-
h2^2)+Qbar26(1)*(h4^2-h3^2));
B66=1/2*(Qbar66(1)*(h1^2-ho^2)+Qbar66(2)*(h2^2-h1^2)+Qbar66(2)*(h3^2-
h2^2)+Qbar66(1)*(h4^2-h3^2));
```

```
D11=1/3*(Qbar11(1)*(h1^3-ho^3)+Qbar11(2)*(h2^3-h1^3)+Qbar11(2)*(h3^3-
h2^3)+Qbar11(1)*(h4^3-h3^3));
D22=1/3*(Qbar22(1)*(h1^3-ho^3)+Qbar22(2)*(h2^3-h1^3)+Qbar22(2)*(h3^3-
h2^3)+Qbar22(1)*(h4^3-h3^3));
D12=1/3*(Qbar12(1)*(h1^3-ho^3)+Qbar12(2)*(h2^3-h1^3)+Qbar12(2)*(h3^3-
h2^3)+Qbar12(1)*(h4^3-h3^3));
D16=1/3*(Qbar16(1)*(h1^3-ho^3)+Qbar16(2)*(h2^3-h1^3)+Qbar16(2)*(h3^3-
h2^3)+Qbar16(1)*(h4^3-h3^3));
D26=1/3*(Qbar26(1)*(h1^3-ho^3)+Qbar26(2)*(h2^3-h1^3)+Qbar26(2)*(h3^3-
h2^3)+Qbar26(1)*(h4^3-h3^3));
D66=1/3*(Qbar66(1)*(h1^3-ho^3)+Qbar66(2)*(h2^3-h1^3)+Qbar66(2)*(h3^3-
h2^3)+Qbar66(1)*(h4^3-h3^3));

El=Q11;
Vstif=114034e-9;
Vs=pi*((a+t).^2-a^2)*L;
Vt=Vstif+Vs;
theta11=[30]*pi/180;
for kkk=1:1;
c=cos(theta11(kkk));
s=sin(theta11(kkk));

A11_s=El*A*2*(c^3)/aa;
A12_s=El*A*2*(s^2)*c/aa;
A22_s=El*A*(2*s*s*s+2)/b;
A66_s=El*A*2*s*s*c/b;

B11_s=A11_s*t(o)/2;
B12_s=A12_s*t(o)/2;
B22_s=A22_s*t(o)/2;
B66_s=A66_s*t(o)/2;

D11_s=B11_s*t(o)/2;
D12_s=B12_s*t(o)/2;
D22_s=B22_s*t(o)/2;
D66_s=B66_s*t(o)/2;

x=[0.19 0.28 0.43 0.54 0.61 0.66 0.7 0.76] ;
C11=(x(o)*A11+(1-x(o))*A11_s);
C12=(x(o)*A12+(1-x(o))*A12_s);
C22=(x(o)*A22+(1-x(o))*A22_s);
C33=(x(o)*A66+(1-x(o))*A66_s);
C14=(x(o)*B11+(1-x(o))*B11_s);
C24=(x(o)*B12+(1-x(o))*B12_s);
C36=(x(o)*B66+(1-x(o))*B66_s);
C15=C24;
C25=(x(o)*B22+(1-x(o))*B22_s);
C44=(x(o)*D11+(1-x(o))*D11_s);
C45=(x(o)*D12+(1-x(o))*D12_s);
C55=(x(o)*D22+(1-x(o))*D22_s);
C66=(x(o)*D66+(1-x(o))*D66_s);

for nn=1:100;
   for m=1:100;
      M=pi*m/L;
      N=nn/a/2;
a11=2*C11*(M^2)*a+2*C33*(N^2)*a;
```

```
a12=2*C12*M*N*a+2*C33*N*M*a;
a13=-(C14*M^3*a+2*C12*M+2*C24*M*N^2*a);
a22=2*C22*N^2*a+2*C33*(M^2)*a;
a23=-(C22*N+2*C24*M^2*N*a+C25*N^3*a);
a33=2*C22/a+4*C24*M^2+2*C55*N^4*a+2*C25*N^2+2*C44*M^4*a+8*C66*M^2*N^2*a+4*C45
*M^2*N^2*a;
P=pi*(a11*a22*a33+2*a12*a13*a23-a11*a23^2-a12^2*a33-a13^2*a22)/(M^2*(-
a12^2+a11*a22));

p(nn,m)=P*1e9;
%p1(n,m)=P1*1e9;
end;
end;
PP=[];

for i=1:100;

   %P3=p1(i,1:100);
   P2=p(i,1:100);
   PP=[P2 PP];
   %PPP=[P3 PP];
end;
kk=sort(PP);
%kkk=sort(PPP);
kk(1:20);
%kkk(1:50)
P_a(o,kkk)=kk(1);
end;
end;
P_a
```

VITA

Samuel Kidane was born in Ethiopia in 1974. He received his Bachelor of Science degree in mechanical engineering in 1997 from Addis Ababa University, Ethiopia. After graduation he was employed as a Technical Officer in Ethiopian Shipping Lines Company. After one year and a half he joined Shell Ethiopia Ltd., and served as lubricants engineer for another year and a half.

In August 2000 he came to the United States and joined Louisiana State University to pursue a Master of Science degree in mechanical engineering. There he studied mechanical systems under the Mechanical Engineering Department and expects to receive a degree of Master of Science in August 2002. During his master's study, he served as a research assistant and was also a teaching assistant for courses such as dynamics, kinematics, and materials engineering.

Samuel Kidane is an active member of the Ethiopian Society of Mechanical Engineers and the American Society of Mechanical Engineers.